Changes in the future summer Mediterranean climate: contribution of teleconnections and local factors.

Monika J. Barcikowska[1], Sarah B. Kapnick[2], Lakshmi Krishnamurty[3], Simone Russo[4], Annalisa Cherchi[5], Chris K. Folland[6,7,8]

[1]Environmental Defense Fund, New York City
[2]Geophysical Fluid Dynamics Laboratory, National Oceanic and Atmospheric Administration, 201 Forrestal Road, Princeton, NJ 08540, USA
[3]Princeton University, GFDL Princeton University Forrestal Campus, 201, Forrestal Road, Princeton, NJ 08542, USA
[4]Institute for Environmental Protection and Research (ISPRA), Rome, Italy
[5]Fondazione Centro Euro-Mediterraneo sui Cambiamenti Climatici, and Istituto Nazionale di Geofisica e Vulcanologia, Bologna, Italy
[6]School of Environmental Sciences, University of East Anglia, Norwich, UK
[7]Department of Earth Sciences, University of Gothenburg, Sweden
[8]International Centre for Applied Climate Sciences, University of Southern Queensland, Australia

Abstract

This study analyzes future climate for the Mediterranean region, projected with the high-resolution coupled CM2.5 model, which incorporates a new and improved land model (LM3). The simulated climate changes suggest pronounced warming and drying over most of the region. However, the changes are distinctly smaller than those of the CMIP5 multi-model ensemble. In addition, the changes over much of southeast and central Europe indicate very modest warming compared to the CMIP5 projections and also a tendency to wetter conditions. These differences indicate a possible role of factors such as land surface-atmospheric interactions in these regions. Our analysis also highlights the importance of correctly projecting the magnitude of changes in the summer North Atlantic Oscillation, which has the capacity to partly offset anthropogenic warming and drying over the western and central Mediterranean. Nevertheless, the projections suggest a decreasing influence of local atmospheric dynamics and teleconnections in maintaining the regional temperature and precipitation balance, in particular over arid regions like the eastern and southern Mediterranean, which show a local maximum of warming and drying. The intensification of the heat low in these regions suggests rather an increasing influence of warming land surface on the local surface atmospheric circulation and progressing desertification.

1. Introduction

The climate in the Mediterranean region is primarily characterized by mild, wet winters and hot, dry summers. However, the complex geomorphological characteristics including gulfs, peninsulas, islands, the mountain ridges surrounding the Mediterranean Sea basin, as well as the influence of the mid-latitude and tropical atmospheric circulation patterns translate into a distinctively complex climate.

The influence of the mid-latitude circulation on the regional hydroclimate is mostly manifest in the teleconnection with the North Atlantic Oscillation (NAO, e.g. Hurrell, 1995, Krichak et al., 2002, Barcikowska et al., 2017b). The summer expression of the NAO (SNAO, Folland et al., 2009, Linderholm et

al., 2009, Blade et al., 2012), in its positive phase yields a stronger meridional sea level pressure (SLP) gradient over the North Atlantic, an enhanced anticyclonic southern lobe with dry conditions over northwest Europe and rather wet conditions over the central Mediterranean. The SNAO has been linked to the Atlantic Meridional Oscillation (Knight et al., 2006, Folland et al., 2009, Linderholm and Folland 2017), which originates from both internal ocean variations (Knight et al., 2005, 2006, Delworth and Mann 2000; Enfield et al., 2001), and anthropogenic sources (Rotstayn and Lohman, 2002, Mann and Emanuel, 2006). However, current literature has not yet reached a full consensus on the spatial definition (fingerprint), origin and impacts of the SNAO. The results of observational analysis vary, depending on the chosen data set, period, summer season interval, and the analysis method (Barnston and Livezey, 1997; Hurrell and van Loon, 1997, Hurrell and Folland, 2002; Hurrell et al., 2003, 2009, Cassou et al., 2005, Folland, 2009, Blade et al., 2012). This sensitivity stems largely from the pronounced interannual-to-multidecadal variability of the observed SNAO.

In the summer, the northward shift of the Hadley cell reveals a connection between the hot and arid eastern part of the Mediterranean and the Asian and African monsoons, as well as a possible connection between these two monsoons (Rodwell and Hoskins, 1996, Ziv et al., 2004, Fontaine et al., 2011, Raicich et al., 2003, Rowell, 2003). Thermal balance of the central-eastern part of the Mediterranean is largely maintained by the two dynamical factors, i.e. the cool air advection of the low-level northerly winds (i.e. Etesians; HMSO, 1962; Metaxas, 1977, Maheras, 1980; Prezerakos, 1984; Reddaway and Bigg, 1996; Zecchetto and de Biasio, 2007; Chronis et al., 2011) and the adiabatic warming of the mid- and upper level subsidence winds (Raicich et al., 2003, Mariotti et al., 2002, Tyrlis et al., 2013), which counterbalance each other. Ziv et al., (2004) have shown these two factors to be significantly correlated, pointing to the Asian Summer Monsoon which exerts an influence on the Mediterranean surface-, mid- and upper-troposphere dynamics. The possible mechanism behind this linkage was explored in a framework of the Rossby wave pattern response to the diabatic heating of the monsoon convection, i.e. monsoon-desert mechanism (Rodwell and Hoskins, 1996, Tyrlis et al., 2013, Rizou et al., 2015, Cherchi et al., 2014, Cherchi et al., 2016). Additionally, Rodwell and Hoskins, 2001 explained changes of Etesian winds as a direct result of changes in the subsidence over the eastern Mediterranean, which via Sverdrup's equation controls the low-level northerly flow.

The geographic location and socio-economic state of the Mediterranean make the population in this region particularly vulnerable to climate change. The southern part of the Mediterranean, which is dominated by agricultural activities, is especially sensitive to prolonged water shortages and their consequences, such as drought and wildfires. Giorgi (2006) found this region to be particularly responsive to projected climate change and identified it as a climate hot spot. In fact, both CMIP3 (Giorgi and Lionello, 2008, Hanf et al., 2012) and CMIP5 future projections for this region (Diffenbaugh and Giorgi, 2012, Alessandri et al., 2014, Mariotti et al., 2015, Feng et al., 2014) indicate very strong warming and reductions in precipitation during the summer season. These changes can increase aridity of the region and hence severely impact water and food security.

However, some studies (e.g. Christensen and Boberg, 2012, Mueller and Seneviratne, 2014) indicated that the projected in CMIP3 and CMIP5 future warming is spuriously amplified by a strong summertime positive bias in land surface temperature, caused by the deficiencies in the simulated atmosphere - land surface feedbacks. Soil moisture-temperature feedbacks were identified as a dominant factor controlling summer temperature variability in the Mediterranean and central Europe in a changing climate (Seneviratne et al. 2006), including the projected and observed amplification of warming hot extremes (Diffenbaugh et al., 2007, Hirschi et al. 2011). Berg et al. 2016 have shown that projected reductions in soil moisture diminish the positive trends in latent heat fluxes over land, which enhances sensible heat fluxes, thereby increasing land surface temperatures

and its aridity. Global coupled models like those used in CMIP and in the present study do not include dynamic irrigation, changes in water management may alter availability of surface water and in offline modeling have been shown to have regional cooling effects (Sacks et al. 2009). Hence, simulating future climate changes in the Mediterranean requires a good understanding of land hydrology, land use, and associated land-atmosphere feedbacks.

Cherchi et al. (2016) also found that the projected in CMIP5 future severe warming over the eastern Mediterranean cannot be explained with the impact of South Asian monsoon teleconnection, maintained via monsoon – desert mechanism alone. On the other hand, Blade et al. (2012) argued that the regional warming and drying projected in CMIP3, is caused by the misrepresentation of the summer NAO teleconnection. Kelley et al. (2012) indicated that CMIP5 models show a rather modest improvement in the simulated regional hydroclimate, compared to CMIP3. The CMIP5 historical simulations still differ from the observations, for example by showing a strong wetting over the northwestern parts of Europe and drying over the southwestern parts of the Mediterranean (e.g. Kelley et al., 2012), though some earlier lower resolution models do show strong drying over many, though not all, parts of north west Europe as well (e.g. Rowell and Jones, 2006). The inconsistencies found between the observations and simulations do not add to the credibility of the current future projections for the Mediterranean and prompt further investigation, using higher resolution models and also advanced understanding of the land surface–atmosphere feedbacks as well as the regional teleconnections.

In this study we analyze the future summer climate over the Mediterranean, projected with the GFDL CM2.5 model (Delworth et al., 2012). It incorporates higher spatial resolution (~50km) and an improved land model (LM3) with enhanced hydrology and associated land-atmospheric feedbacks (Milly et al., 2014). This likely improves the simulated hydroclimate and temperature over many continental regions including Europe (Delworth et al., 2012). The analysis aims to interpret the derived future climate changes through the prism of contributing SNAO teleconnection, as well as the impact of local surface warming and the associated land surface-air interactions.

Section 2 describes the model and experiments used, the dataset for comparison and the methodology. Section 3 focuses on the summer time-mean climatology of the region, as well as its teleconnections. It evaluates the performance of the model in terms of the simulated regional precipitation, as well as large-scale circulation features, which shape the summer regime of the Mediterranean climate. It also examines the capacity of the model to simulate the SNAO and its impact on the Mediterranean climate. The last part of this section focuses on a representation of the key dynamical features of the eastern Mediterranean climate, i.e. the linkage between the mid- and upper-level subsidence and the low-level northerly flow (and the associated Etesian winds) together with its coupling with the Indian Monsoon. Section 4 investigates future climate changes over the Mediterranean derived from the model projections. It examines the regional changes from the perspective of a) large-scale circulation over the Euro-Atlantic and the influence of the SNAO teleconnection, b) local land surface warming and its influence on the climate regime of the eastern Mediterranean. Section 5 discusses and summarizes the main results.

2. Data and Methods

2.1 Coupled model and experiments

The coupled model used in this study is the Geophysical Fluid Dynamics Laboratory (GFDL) CM2.5. It has an atmospheric and land surface horizontal grid scale of approximately 50 km with 32 levels in the vertical. The horizontal grid scale of the ocean increases from 28 km in the tropics to 8-11 km in high latitudes. CM2.5

incorporates a new land model (LM3) of land water, energy, and carbon, with enhanced representation of soil moisture and land-atmospheric feedbacks between soil moisture and precipitation (Milly et al., 2014, Berg et al., 2016). Details of the CM2.5 model features can be found in Delworth et al. (2012). The representation of the summer precipitation climatology in CM2.5 is also compared using a 4000-years control run of GFDL CM2.1, that is the CM2.5's predecessor. CM2.1 incorporates a grid scale of 2° latitude x 2.5° longitude for the atmosphere. The ocean resolution is variable being approximately 1° latitude x 1° longitude, with a finer meridional resolution in the tropics. The CM2.1 atmospheric model has 24 vertical levels (Delworth et al., 2006). The ocean component CM2.1 and CM2.5 consist of 50 levels in the vertical. Future changes projected with CM2.5 are compared with that derived with the CSIRO-Mk3-6-0 model (1.9° x 1.9° horizontal resolution for the atmosphere), which includes the ocean component based on the GFDL ocean model. This choice was determined by the fact that future projections of CSIRO-Mk3-6-0 model, unlike CM2.1, follow the same protocol of forcing scenario, i.e. the IPCC RCP8.5 scenario (Meinshausen et al. 2011, Riahi et al., 2011), as those of CM2.5.

The set of experiments performed using CM2.5 are listed in Table 1 and it consists of control simulations (hereafter CTRL) and 5-members ensembles of historical simulations (hereafter HIST), and of future projections (hereafter PROJ) performed with CM2.5. The CTRL simulation consists of a 1000-year integration, where greenhouse gas and aerosol compositions are held fixed at the levels of the year 1860. In HIST and PROJ ensembles, the forcing follows the protocols of the Coupled Model Intercomparison Project Phase 5 (http://cmip-pcmdi.llnl.gov/cmip5/forcing.html). For the historical period (1861-2005), the radiative forcings are based on observational estimates of concentrations of well-mixed greenhouse gases (GHG), ozone, volcanoes, aerosols, solar irradiance changes and land-use distribution. While for the future (2006-2100) the radiative forcing follows an estimate of projected changes defined in the IPCC RCP8.5 scenario. This scenario assumes high population growth, slow technological change and energy intensity improvements, and a lack of developed climate change policies, resulting in large energy demand and GHG emissions.

2.2 Datasets used for comparison

The simulated features of large-scale circulation are compared with reanalysis data of monthly pressure at mean sea-level (hereafter SLP), wind vectors at the 850hPa and 200hPa levels, and vertical velocity at 200hPa for the period 1979-2017. Reanalysis data is provided by the NCEP-DOE AMIP-II Reanalysis 2 (hereafter NCEP-DOE2) with 2.5° x 2.5° horizontal resolution and 17 vertical levels (Kanamitsu et al., 2002; https://www.esrl.noaa.gov/psd/data/gridded/data.ncep.reanalysis2.html).

The simulated precipitation is compared with the seasonal time-averaged precipitation provided by the University of Delaware (V4.01), Legates and Willmott 1990; http://climate.geog.udel.edu/~climate/html_pages/README.ghcn_ts2.html (last access: July 2018). This is a global gridded land data set with 0.5° x 0.5° horizontal resolution for the period 1980-2015. For the same period we use also EOBS precipitation data set provided E-OBS dataset from the EU-FP6 project UERRA (http://www.uerra.eu) and the Copernicus Climate Change Service (Cornes et al. 2018, version 17), provided at 0.25° x 0.25° horizontal resolution.

The observational analysis of the summer North Atlantic Oscillation (section 3.2) is carried out using July-August mean sea level pressure (SLP), provided by NOAA/ESRL PSD 20th Century Reanalysis version 2c (Compo et al. 2006, https://www.esrl.noaa.gov/psd/data/20thC_Rean/). The spatial patterns of the dominant component of the SLP variations are computed with Empirical Orthogonal Function (EOF) analysis, over the

domain [25°-70°N, 70°W-50E°], following Folland et al., 2009. The robustness of the pattern is tested against chosen periods of different length.

2.3 Analysis methods

The representation of the simulated large-scale atmospheric circulation over the Mediterranean (section 3.1) is analyzed using CTRL runs' monthly mean fields of the lower, mid- and upper- level dynamics over the region covering southern Europe, North Africa and South Asia [30°N–50°N, 30°W–110°E]. The analysis of the simulated SNAO teleconnection focuses on the Euro-Atlantic region. In the analysis of the eastern Mediterranean climate, we define the region of focus as EMED [30°-36°N, 36°-42°E]. We will also refer to the eastern Mediterranean land region, which includes: Syria, Lebanon, Israel, Jordan, as the Levant region.

The time-mean large-scale circulation features are analyzed based on the monthly means of hydro-meteorological variables for the summer (June, July and August, hereafter JJA) season. Future changes are estimated by comparing the climatology at the end of the twenty-first century (i.e. 2061–2099, hereinafter future) of the RCP8.5 scenario with that at the end of the twentieth century (i.e. 1961– 1999, hereinafter present) of the historical simulation using monthly mean fields for the summer season.

The teleconnection of the Mediterranean climate with SNAO is analyzed using the full (1000 year) CTRL run (section 3.2), as well as the historical and future runs. The SNAO is defined as a lead component of SLP vector time series over the Euro-Atlantic region [25°N–75°N, 70°W–50°E] in "core summer" (July-August), following Folland et al. 2009. The choice of the time window is determined by the fact that the temporal behavior of the SNAO in significantly correlated only within these two months. The impact of this teleconnection on Mediterranean climate is estimated using correlations between SNAO PC time series and the regional temperature and precipitation, using the long CTRL experiments and the historical and future ensembles. The evolution of the SNAO fingerprint in the 20^{th} and 21^{st} century is analyzed by projecting the vector time series of HIST and PROJ experiments (240 yrs, 1861-2100) on the SNAO eigenvector derived from the CTRL run. To analyze potential changes in the spatial pattern of SNAO and associated impacts, the EOF analysis is applied independently to each of the HIST and PROJ ensembles, in the period 1950-2010 and 2040-2100, respectively, detrending the time series before computing the EOF. In both epochs, the analysis has been also tested for shorter periods (i.e. 50 and 30 years), which did not change the results in qualitative terms. Each of the five SNAO time series for the 1950-2010 and 2040-2100 periods was correlated with the respective detrended precipitation fields. The results are compared with the observational analysis, using SLP provided by the 20CR dataset in the period 1870-2010.

The summer climate regime of the eastern Mediterranean (EMED) is examined from the perspective of the regional mid- and upper-tropospheric subsidence and its physical linkage with the surface circulation (section 3.3). The seasonal variability of the subsidence over the eastern Mediterranean is derived from EOF analysis applied to vertical velocity (omega) fields at 500 hPa, and also at 300 hPa (each level separately) over the region covering the Mediterranean, North Africa and the Middle East in July season. The physical linkage between the subsidence and surface circulation is estimated using correlations between the time series of the first EOF component (PC1) and the regional sea level pressure, geopotential height and wind vectors at 850 hPa. The relationship between the EMED region dynamics and the Indian Summer Monsoon (ISM) is estimated by computing additional correlations with precipitation, outgoing longwave radiation, and the vertically integrated water column. The analysis shows the correlations computed using time series of EOF omega at 500 hPa, but the correlations using EOF omega at 300 hPa were almost the same. The results of the

analysis are shown for July when the magnitude of subsidence and the Etesians is at its maximum and the response of the Rossby waves to monsoon rainfall is also strongest (Tyrlis et al. 2012, Lin et al., 2007, Lin et al., 2009). The results derived for June and August are shown in the Supplementary Information.

Future changes in the dynamical linkages governing the summer climate regime over the eastern Mediterranean were analyzed by comparing the five-decade-long samples for July, i.e. 1960-2010 and 2050-2100. The linkage was calculated in a similar manner to that of the control run using correlations between the time series of the EOF over the EMED region subsidence and the atmospheric surface circulation fields. All EOF time series were computed by projecting the respective run on the eigenvector derived from the control run. The correlations were derived for each run (historical and future, respectively), using a priori detrended time series. The final result shows the ensemble mean for the five-member historical and future correlations.

An additional analysis investigates the potential influence of the local EMED temperature on the derived local dynamical relationships (section 4.3 and Supplementary Material). Therefore, the derived correlations were differentiated between samples with the 300 warmest and the 300 coldest summers (July) over the Mediterranean, chosen from the control run time series. Their selection is based on surface temperature in the EMED region. Additionally, a diagnosis of temperature impacts on the regional atmospheric circulation was performed using composite differences between the two temperature samples and the associated relative humidity, sea level pressure, wind components, geopotential height, vertical velocity and precipitation. The results were corroborated by testing their sensitivity to the precise choice of the region.

3 Summer mean present climate and teleconnections over the Mediterranean region

3.1 Simulated summer mean Mediterranean climate

Figure 1a,b demonstrates that the model captures the subtropical low-tropospheric circulation with high fidelity when compared with the reanalysis (NCEP-DOE2). It reproduces accurately the zonal pressure gradient over the Mediterranean, both in terms of pattern and magnitude, forged by the difference between the subtropical anticyclone over the North Atlantic and the massive Asian monsoon heat low. The latter extends westward, through the Arabian Peninsula towards the Levant region and southern Asia Minor. Concomitant to the zonal pressure gradient and adjustments to the regional orography is a persistent west-northerly flow over the central and eastern Mediterranean (i.e. the Etesian winds). The model realistically captures its local-scale features, created by adjustments to the regional topography. This includes a local wind maximum centered over the Aegean Sea and its southern extension reaching the Sahel region. These northerlies are also channeled through the Red Sea Straits and the Persian Gulf, reaching the Indian Ocean.

Figure 1c,d shows that the model reproduces the location and magnitude of the summer subtropical mid-troposphere anticyclone, which spreads from the eastern Mediterranean across South Asia. The simulated mid-troposphere also captures the location and a realistic magnitude of the persistent mid-troposphere (500 hPa) subsidence (positive omega) which creates the exceptionally hot and arid climate of the eastern Mediterranean. This subsidence gradually decreases towards the Iranian Plateau, which together with ascending motion over the South Asian monsoon region, creates a large-scale time-mean zonal gradient. The simulated zonal gradient is well shown (Figure 2a) by a vertical cross-section of vertical velocity (omega) averaged over 20°-34°N between the east Mediterranean region (positive omega means enhanced subsidence) and the South Asia (negative omega means ascending air). This characteristic gradient agrees well with its observational counterpart (Figure 2b) both in terms of magnitude and pattern. Importantly, the model captures

the observed local maximum of the eastern Mediterranean subsidence located at middle-tropospheric levels (300-700 hPa), the region most sensitive to the impact of the Indian monsoon teleconnection.

Figure 3 shows climatologies of the Mediterranean precipitation provided by the observations, the CM2.5 control run, and also its low-resolution (CMIP3) predecessor, i.e. CM2.1 at their original horizontal resolutions. Globally, CM2.5 has been shown to represent temperature and precipitation better than almost every CMIP5 model (Knutti et al. 2013). Regionally, we compare CM2.1 with CM2.5 to understand a representation of differences in precipitation with resolution enhancement and all else equal. Although both CM2.1 and CM2.5 depict the general spatial features of the climatology (i.e. large values in the northern Mediterranean, particularly over the Alps and the Balkans), the former introduces large biases (up to 50%) in the regions with sharp spatial gradients. CM2.5 reproduces precipitation with a greater level of detail, clearly indicating the advantages of higher horizontal model resolution for regions with complex orography. However, precipitation magnitude in most mountainous areas, e.g. the northern Iberian Peninsula, the Alps and over Asia Minor, is larger than in observational data sets, like U. Delaware and EOBS. The climatology in CM2.5, in terms of pattern and magnitude, seem to be more consistent with the EOBS data set. However, due to a relatively large observational uncertainty in many mountainous areas leading to underrepresentation of precipitation over complex terrain in gridded observational datasets, it is difficult to validate the model rainfall climatology in the region (Lundquist et al. 2019). The CM2.5 results are comparable to the downscaling simulations using high - resolution (at ~50 km and ~ 12 km) regional climate models of the EURO-CORDEX experiment (Jacob et al., 2014). Kotlarski et al. (2014) demonstrate that the regional models capture realistic features of the European climate. However, the majority of the experiments feature wet bias over most regions of Europe. This includes, similar to CM2.5, wet bias over the Iberian Peninsula, Balkans and Asia Minor, although some of the models exhibit also dry bias over southeastern Europe. Moreover, increasing spatial resolution from 50km to 12km yielded usually higher precipitation amounts, thereby enhancing the wet bias (Kotlarski et al. 2014).

Overall, our analysis indicates that the high-resolution CM2.5 control run faithfully reproduces the mean surface- and upper-tropospheric circulation over the Mediterranean and it captures the complexity of the regional precipitation found in similar resolution observations (Figure 3). Increasing horizontal atmospheric resolution from 200 km in CM2.1 (approximately the average of CMIP5 models) to 50 km in CM2.5 improves the representation of mountains and coastlines (Kapnick et al. 2014, Delworth et al. 2012), which are necessary to improve regional precipitation, land-ocean dynamics, and regional circulation (Pascale et al. 2016).

3.2 The impact of the summer North Atlantic teleconnections on the Mediterranean region

The imperative of the following section is to test the capability of the model to simulate the SNAO as an independent, internally generated climate component, which would prove the physical validity of the statistically - derived component, following the methodology described in section 2.3. However, allowing for the fact that a) circulation over the SNAO region is influenced by different key factors at different times, giving rise to time-varying dominant modes of apparent internal variability; and b) each simulation represents a different, non-deterministic state of internal climate variations, one should not expect to obtain from each run a replica of the observed SNAO component.

3.2.1 Spatial pattern of SNAO

The EOF analysis applied to the CTRL run (Table 1) results in two modes: the first mode (CTRL EOF1) represents the SNAO and dominates the summer SLP variations, explaining twice as much total variance as CTRL EOF2 (34% and 15%, respectively).

Figure 4a depicts the spatial pattern of CTRL EOF1. The derived dipole resembles the observed SNAO signature (e.g. Folland et al. 2009), including a distinct northward shift when compared to the winter counterpart (shown e.g. in Barcikowska et al. 2017). The dipole pattern has a northern lobe over the south-western flank of Greenland and a southern lobe centered north of the Azores in the vicinity of ~45°N, 30°E. At its positive phase SNAO is manifest with negative anomalies in the former and positive anomalies in the latter region, thereby strengthening the meridional SLP gradient over the North Atlantic. The pattern is similar also when analyzed for the single months of July and August (not shown).

Further analysis indicates also that the signature of the simulated SNAO is much more consistent with the observed one before the 1970s, rather than in the recent six decades. The analysis of EOF1 derived from the consecutive periods of 20CR reanalysis (50-yr periods i.e. a. 1870-1920, b. 1900-1950, c. 1940-1990, d. 1960-2010 in Figure 5; and 40-yr periods, i.e. 1851-1890, 1891-1930, 1931-1970, 1971-2010 in Figure SI1), suggests an evolution of the SNAO fingerprint in time. The patterns observed in the early observational period (1870-1920 and 1900-1950 in Figure 5a,b) bear very strong resemblance to the one simulated in the CTRL EOF1 (Figure 4a), i.e. including the northern centers of action at southern Greenland and with the southern lobe located north of the Azores (~45°N, 35°E). In contrast, the EOF derived for the recent decades (e.g. 1960-2010 or 1971-2010) exhibits a weak northern lobe and a much stronger southern lobe, with the latter being also shifted north-east, towards the British Isles. These differences are also consistent with other observational analysis of the recent six decades (Blade et al., 2012, and Syed et al., 2012).

A similar evolution of the SNAO pattern is found in 4 out of the 5 HIST members available when comparing the early observational periods with the most recent decades (Figure 5b,h; Figure SI2). For example, the pattern derived from all the HIST runs in the period 1870-1920 (Figure SI2, Figure 5b) resembles both the one derived from the observations (Figure 5a) and the one derived from the CTRL run (Figure 4a). In the most recent period (i.e.1960-2010, Figure SI2), the SNAO fingerprints simulated in HIST runs and the observed ones feature a much weaker northern lobe, and the southern lobe shifted north-eastward, towards the British Isles. This tendency intensifies even more when the more recent period is extended towards the future using PROJ members (e.g. 1970-2030, 1970-2060 Figure SI3). As the anthropogenic forcing is the only deterministic factor in the HIST and PROJ experiments, the above results highlight its potential importance in shaping the SNAO and hence explaining to some degree the temporal evolution of its spatial signature in the 20th century.

3.2.2 Impact of SNAO on the Mediterranean climate

The SNAO simulated in CM2.5 exerts an impact on the precipitation, surface temperature and geopotential height over the North Atlantic and Europe (Figure 4), which strongly resembles its observational counterpart (e.g. Folland et al., 2009, Blade et al., 2012). This includes a distinct tripolar pattern of precipitation anomalies with the lobe over southern Greenland, over northern Europe and its vicinity over the North Atlantic, and southern Europe (Figure 4c). The location corresponds closely with the fingerprint of anomalous surface temperature (Figure 4b).

The derived SNAO teleconnection at its positive (negative) phase, manifested in the positive (negative) SLP anomalies over its southern lobe (Figure 4a), is linked with an anomalous warming and drying (cooling, wetting) over northwestern Europe, and anomalous cooling and wetting (warming, drying) over the Mediterranean (Figure 4b,c). Consistent with the observations (Folland et al., 2009) the impact on the former region is almost twice as much stronger than on the latter, both in terms of precipitation and temperature. For example, the magnitude of correlation coefficients in the vicinity of the southern SNAO lobe (i.e. southwest of the British Isles) exceeds about 0.6 for precipitation and 0.5 for temperature, but in the Mediterranean, it remains below 0.35 and 0.4, respectively for precipitation and temperature.

The SNAO teleconnection to the northern and southern parts of Europe points also to different physical mechanisms. While the impact of the SNAO on northern Europe has been straightforwardly explained with changes in the North Atlantic storm tracks (Folland et al., 2009), the impact on the southern Europe hydroclimate (shown in observations by Linderholm et al., 2009) is manifest through the changes in the mid- and upper-tropospheric geopotential height. The correlation analysis between the SNAO time series and 500 hPa geopotential height (Figure 4b, contours), yields a tripolar structure, with the positions of the nodes being well collocated with those of precipitation and temperature. Hence, the negative correlations of geopotential height found over the Mediterranean provide a plausible explanation for the regional precipitation anomalies during the positive SNAO phase, which links to the local effects of anomalous mid- and upper tropospheric trough, associated cooling, and intensified potential instability over the Mediterranean.

3.3 Summer climate regime over the eastern Mediterranean

In this section, we investigate the ability of CM2.5 to simulate the key features shaping the hot and arid climate of the eastern Mediterranean (EMED, as defined in Sect. 2). This comprises a) the linkage between the surface and the mid- and upper-tropospheric dynamics, which maintains the thermal balance of the region; and b) the teleconnection with the Indian Summer Monsoon (hereafter ISM).

The connection between the mid- and upper-tropospheric subsidence and surface circulation over EMED (Figure 6) is depicted with correlations between time series of the dominant EOF of vertical velocity (omega) at 500 hPa (i.e. EOF1 in Figure 6a) and geopotential height and wind vector at 850 hPa, outgoing longwave radiation and precipitation. The EOF pattern is almost identical to the simulated and observed climatology, featuring a monopole pattern being well collocated with the local maximum of subsidence in the vicinity of Crete (Tyrlis et al 2012, Ziv et al. 2004). The EOF persists as a dominant component up to the upper-troposphere (~200 hPa), explaining between 33% -35% of the total variance. Figure 6b,c shows that CM2.5 skillfully captures the connection between the strengthening mid- and upper-tropospheric subsidence and the intensifying Etesians, zonal pressure gradient and concomitant anticyclonic circulation in the central Mediterranean. Consistent with the impact of the adiabatic descent (and associated radiative cooling in dry regions under clear sky conditions), these changes are also manifest in the larger outgoing long-wave radiation and to a smaller degree in reduced precipitation (Figure 6e,f). The simulated in CM2.5 relationship closely resembles its observational counterpart, derived by correlating the regional anomalies of omega 500 hPa and meridional wind using the detrended NCEP–DOE2 data set, shown in Figure 6d.

The correlations derived between the omega and monsoon indices (Figure 6) suggest that the model reproduces the impacts of the Indian summer monsoon (ISM) teleconnection, consistent with the previous modeling and observational studies (Hoskins et al., 1996, Hoskins et al., 2001, Tyrlis et al., 2012, Ziv, 2004, Cherchi et al., 2014). The analysis represents the linkage between the strengthening subsidence over the

EMED region and the intensified ISM, depicted here with the negative anomalies of the OLR, positive anomalies of precipitation and vertically integrated water vapor (not shown) centered over the northwestern coast of India. The intensified ISM is congruent with the intensified heat low over the Arabian Peninsula and the Arabian Sea, and the intensified south-westerlies over the Arabian Sea, which feed the monsoon with moisture (Figure 6b, c). As pointed previously in Ziv et al. (2004), the linkage exerts also an effect on the surface circulation over EMED by modulating the intensity of the heat low and hence the intensity of the zonal pressure gradient over the Mediterranean and associated regional northerly flow, i.e. Etesians.

These results suggest that CM2.5 is capable of capturing the most prominent features of the summer climate regime over the eastern Mediterranean. The next section investigates the projected future Mediterranean climate, interpreting this through the prism of the governing factors, i.e. large-scale circulation, local relationships and teleconnections.

4. Climate changes in the 21st century

4.1 Comparison of future and present summer climate

CM2.5 projections of future large-scale circulation over the Euro-Atlantic region are largely consistent with those seen in the CMIP3 and CMIP5 simulations. The most prominent feature of the derived changes is a northward shift and strengthening of the North Atlantic meridional SLP gradient. This pattern, manifest as an SLP dipole with cyclonic anomalies centered over Greenland and anticyclonic anomalies centered southwest of the British Isles, is a typical fingerprint of anthropogenic climate change (Collins et al., 2013). The anthropogenic fingerprint closely resembles the CTRL-based SNAO at its positive phase (despite a slight shift northeast of the CRTL SNAO), thereby suggesting a possible contribution of the anthropogenic component towards positive tendencies of the future SNAO, similarly to what found by Folland et al. (2009) for HadCM3 and HadGEM1.

Figure 7 indicates a very strong warming reaching locally 7°C (in JJA during the whole day), and an intensification of the thermal low over the Sahara, the eastern Mediterranean and the Arabian Peninsula. The local maximum of the warming, located over the Levant and inland Arabian Peninsula, collocates well with an anomaly of convergent flow and ascending air, expanding from the surface up to mid-tropospheric levels (Figure 2c, Figure SI4), and thereby intensifying the Persian trough. The latter contributes to the weaker subsidence in the eastern Mediterranean and, together with an intensified subsidence over the central Mediterranean, shifts the local maximum of subsidence towards the northwest.

The projected changes in the circulation over Europe show important differences from the CMIP5 multi-model ensemble of RCP8.5 scenario (Collins et al. 2013) and the CMIP3 ensemble of the A1B scenario (Giorgi and Lionello, 2008), both in quantitative and qualitative terms. The changes simulated in CM2.5 can be largely described as a transition zone between the intensifying anticyclonic circulation, centered in the vicinity of British Isles, and intensifying thermal low over the eastern Mediterranean and the Middle East. Hence the northwestern and central parts, including the central Mediterranean feature an increase in SLP. Both, the increasing SLP in the central Mediterranean and the decreasing SLP in the eastern Mediterranean amplify the zonal pressure gradient in this region and the concomitant Etesian winds. In contrast, CMIP5 ensemble shows negative SLP anomalies over most of Europe (except the British Isles), which contribute to the weakening of the regional zonal pressure gradient and the associated northerly flow (Collins et al. 2013, Fig 12.18).

The warming projected in CM2.5 shows a stark gradient between the southwestern and northeastern parts of Europe, which is consistent with the CMIP5 and the EURO-CORDEX ensembles. However, for the latter ones, the gradient is weaker and the minimum of warming shifted northward (see Fussel et al. 2017, Map3.4; Figure SI6), i.e. located over the southeastern Baltic countries. In CM2.5 the minimum of warming is located in the northern Balkans and southeast Europe (Figure 7b), and accompanied with wetting tendencies. For these regions, the projected in CM2.5 warming is strikingly weaker, compared to other ensemble projections. While CM2.5 projects values falling within 0.5-2.5°C the ensemble average of combined GCM–RCM simulations from the EURO-CORDEX initiative (Fussel et al., 2017, Map 3.4, pp. 76) projects warming of 3.5 - 5.5°C. The 10-member RCP8.5 ensemble of the CSIRO-Mk3-6-0 model indicates warming exceeding 6°C (Figure SI5). The warming projected in CM2.5 for the regions such as the Iberian Peninsula, southern France, southern Balkans varies between 3.5 and 6°C, which is still distinguishably lower than in CSIRO-Mk3-6-0, which projects warming between ~5.5-8°C.

CM2.5 features (Figure 7c) a sharp transition zone between the drying in southwestern Europe and the wetting in northeastern Europe. However the gradient in CM2.5, analogously to the temperature changes gradient, is much sharper and the wetting tendencies extend southward (down to northern Balkans) when compared with the CMIP3 and CMIP5 ensemble (Fussel et al. 2017, Map 3.8). Owing to its relatively high resolution, CM2.5 also provides more spatially refined information, which includes, for example, sharper gradients along the coasts or in the mountainous regions. All coastal regions experience reductions in precipitation, expected from the strengthening temperature contrast between the fast warming land and slower warming sea. These reductions are especially pronounced along the northwestern coasts of the Iberian Peninsula, where rainfall is typically larger due to incoming North Atlantic storms.

4.2 Future changes in SNAO-Mediterranean teleconnections

Analysis of the 20th and 21st century simulations exhibits long-term changes in the behavior of the SNAO, both in terms of magnitude and pattern. The temporal evolution of the SNAO, depicted as an ensemble average of the HIST+PROJ runs (Figure 8c), indicates its positive tendencies both in the latter half of the 20th century and the 21st century. However, the trend found for the former period is much weaker and in separate realizations is even hampered by relatively strong interannual- to multi-decadal variations. This is consistent with the SNAO signal observed in the recent decades, which features rich variability across time scales and a relatively weak positive trend, as described in section 3.2.1. For the latter period (particularly 2040-2100) the trend becomes strong enough to be discernible in every realization.

Further analysis points to the subtle changes in the future spatial pattern of the SNAO. Comparison of the SLP fingerprint between 1960-2010 and 2050-2100 (Figure 8a,b) indicates a northeastward shift, thereby making the southern lobe of the SNAO located closer to the British Isles. This feature is also consistent with the projected intensification and northeastward shift of the meridional SLP gradient over the North Atlantic (Figure 7a). The future changes in the SNAO are also discernible in the teleconnection with the European hydroclimate. The comparison of the correlations, derived for the time series of the SNAO component and precipitation anomalies, (Figure 8a,b) indicates a strengthening impact over Europe, i.e. enhanced drying (wetting) in northern Europe and wetting (drying) over southern Europe during the positive (negative) SNAO phase. The changes over the Mediterranean are found mostly over the Iberian Peninsula, southern Balkans and Asia Minor, suggesting that the future intensification of the SNAO may play in these regions an important role in moistening and offsetting the drying effects of the anthropogenic changes.

As shown in the previous section, changes in the seasonal precipitation over the Mediterranean (Figure 7b,c), indicate strong warming and drying. Hence the key implication of these results is that without the SNAO the future climate drying in the Mediterranean would be even more severe. Figure 8d,e depicts the seasonal regional future changes (1961-1999 versus 2061-2099), and the changes without the contribution of the SNAO, that offsets the regional drying. The comparison of the changes indicates that the largest differences are well collocated with the intensified impact of the SNAO (Figure 8a,b). For example, the average drying would intensify from ~-0.4 to -0.65 mm/day (~ 27 to 43 %, please note that the relatively large percentage numbers for this region are partly due to a very low summertime local average precipitation) for the southeast and central Iberian Peninsula, from ~-0.3 to -0.55mm/day (~10 to 18 %) over the Balkan coast, and from ~-0.6 to -0.8 mm/day (~18 to 26 %) for parts of Asia Minor, when the impact of the SNAO is removed. These differences underline the role of the SNAO in shaping the climate of southern Europe.

These results are consistent with Blade et al. 2012, who emphasized the role of the SNAO in offsetting the future drying and warming in the Mediterranean. On the other hand, our results do not support the theory proposed by Blade et al. 2012, that potential deficiencies in the regional impact of the SNAO teleconnection simulated by the CMIP5 model are causing excessive warming and drying in the future projections for the Mediterranean. The impact of the SNAO (in terms of pattern and magnitude) in CM2.5 is almost the same as the one shown for the CM2.1 (Blade et al. 2012) and yet the former projects substantially less intense warming and drying over southern Europe, compared to the latter (Blade et al. 2012), or to the CMIP3 and CMIP5 ensembles (Collins et al. 2013). Moreover, CM2.5 projections for the northern Balkans and central Europe show wetting tendencies, as opposed to drying projected in the CM2.1 runs and CMIP3/CMIP5 ensembles. For these regions CM2.5 projections show also strikingly weaker warming (~0.5 to 2°C), compared to the CSIRO-Mk3-6-0 ensemble (~6-7°C, Figure SI5) or EURO-CORDEX initiative (~3.5-5.5°C, Fussel et al., 2017). However, the impact of the SNAO (observed and simulated in CM2.1 and CM2.5) in these regions is very small or negligible, suggesting that other factors might be responsible for these discrepancies.

4.3 Future changes in the summer regime of the eastern Mediterranean

This section focuses on future changes in the key local features shaping the regime of the EMED climate. This includes an analysis of the stationarity of the local linkage between the low- and mid-to-upper tropospheric dynamics and the influence of the local surface warming on the surface circulation.

4.3.1 Changes in the local linkage shaping the EMED climate regime

Figure 9 compares the HIST and the PROJ five-member ensemble average of the correlations, derived between the regional mid-tropospheric subsidence and the indices of the surface circulation. The comparison of the correlations, which represent the dynamical linkage governing the present and future climate regime over EMED, exhibits qualitative and quantitative differences. For the future period the correlations, estimated for both, the regional surface pressure systems (Figure 9b), the concomitant zonal pressure gradient and the surface northerlies (i.e. Etesians, Figure 9d), are substantially weaker, e.g. by more than a factor of two (from ~0.7 to ~0.3) for the regions of Levant and Persian Gulf. Figure 9c,d also shows that for some regions of North Africa the linkage almost vanishes. This is consistent with the radically reduced correlations estimated for the water vapour and precipitation (from ~0.4-0.5 to ~0) over the African monsoon region (Figure 9e,f), which largely depends on the influx of moisture transported with the northerly flow over EMED and North Africa.

On the other hand, correlations between the EMED subsidence and ISM indices (July), i.e. precipitation and column-integrated water vapour (Figure 9e,f), do not show quantitative differences. The patterns, derived for both variables are slightly shifted towards the southwest in the future period, which is consistent with the changes in the atmospheric circulation supplying the ISM monsoon with moisture.

These results do suggest a pronounced weakening of the local linkage between the mid- and upper-tropospheric subsidence and surface circulation over the EMED. Moreover, given that the local linkage serves as a "medium path" for the teleconnection between the ISM and surface circulation over EMED, future weakening of the local linkage will most likely diminish the impact of this teleconnection on the EMED surface circulation. On the other hand, the projected intensification of the heat low over EMED, North Africa, and the Middle East points to an increasing role of the warming over the arid surfaces. Thus, in the following section, we explore apparent nonlinearities in the summer climate regime of the eastern Mediterranean associated with the local surface temperature.

4.3.2 Nonlinear dependency of the local linkages between the low-tropospheric and the mid-tropospheric dynamics and their contributions to the thermal balance over EMED.

In this section, we focus on the impacts of the warming local surface temperature on the low-level circulation, including the linkage between the low-level and the mid-tropospheric dynamics over EMED. The analysis uses the CTRL run, which excludes the time-varying anthropogenic climate forcing and hence allows us to focus on the natural variability of the system and nonlinear interactions that would be difficult to statistically calculate in shorter HIST runs. As described in section 2, we analyze two samples with 300 cases of the lowest and highest monthly mean temperature in July, with respect to the mean surface temperature over the EMED region.

The following analysis compares the strength of the local linkage between the mid- and upper-tropospheric subsidence over EMED, derived for the sample with the cold and warm temperatures, much as done in the previous section comparing recent historical and future periods. The comparison, consistent with the results shown in previous section (Figure 9), indicates a radical weakening of the linkage derived between the mid-level subsidence over EMED and the zonal surface pressure systems over the central and eastern Mediterranean, Etesian winds and their extension over North Africa and the Persian Gulf, and precipitation over the Sahel (Figure SI6).

Further analysis shows the influence, the warming land over the eastern Mediterranean, exerts on the local circulation. Figure 10 depicts the response of the summer Mediterranean climate to the surface warming over EMED, estimated with composite differences between the two samples (high temperature minus low temperature), in terms of temperature, relative humidity, pressure and wind vector, geopotential height at 500 hPa and 800 hPa, omega at 500 hPa and precipitation. The response (Figure 10c) features bipolar SLP anomalies, with a low-pressure anomaly over North Africa, EMED and the Middle East, and a high-pressure centered over the northern Balkans and the Black Sea. The intensified heat low over the EMED and the Arabian Peninsula (Figure 10c) is in congruence with the enhanced convergence in these regions and the reduced subsidence at the low- and mid-tropospheric levels at 500 hPa (Figure 10e) and 700 hPa (not shown). At the same time, the positive SLP anomalies (Figure 10c) and the increased subsidence over Asia Minor and the Black Sea are physically consistent with increased adiabatic warming and stability, reflected in the maximum of warming, the reduced relative humidity and precipitation. The derived bipolar SLP anomaly

intensifies also the zonal pressure gradient over the central and eastern Mediterranean, which directly translates into the intensified Etesian winds.

The analysis repeated for the July-August season yields similar results, although with a reduced magnitude due to a weaker signal in June and August (Figure SI7).The analysis repeated for the response to the warming over the domains extended towards southern parts of the central and western Mediterranean (Figure SI8a,b) yields qualitatively similar results (i.e. the bipolar SLP anomalies), but with an increased magnitude of the response over the southwestern Mediterranean. On the other hand, analysis repeated for the warming regions confined to the Levant, Arabian Peninsula and Asia Minor and Black Sea (30°-50°E, 30°-45°N, Figure SI8e), shows the pattern with the response (anticyclone anomaly) intensified towards the Middle East. The most similar results are obtained, qualitatively and quantitatively, when the region is confined to the same latitudes but slightly extended towards east and west (30°-50°E, 30°-36°N, Figure SI8c), i.e. centered over the Levant and northern parts of Arabian Peninsula.

Our analysis indicates that the dynamical regime over the EMED largely depends on the local temperature. During relatively cool years the dynamical relationship between the low-level Etesian winds and the mid-level subsidence, which maintains the local temperature balance, seems to be much stronger. During warmer years, this relationship is weaker, which is likely due to the local response in surface circulation triggered by the warming land. The response (i.e. an intensifying heat low, anomalous convergence and very pronounced ascending motion at the low and mid-levels of the EMED and Arabian Peninsula; intensified zonal pressure gradient and Etesians; strong drying over Asia Minor and southern Balkans), is consistent with the anthropogenic changes projected over the Mediterranean (in JJA: Figure 7a,b,c, Figure SI4a,c,e; in July: Figure SI4b,d,f). Overall, this suggests that the importance of the local atmospheric responses, driven by the warming land surface, will have an increasing influence in the future climate of the Mediterranean region.

The analysis, however, does not explain the processes involved in the dipole-like response in the circulation, which comprises SLP, winds and omega anomalies north from the EMED region (particularly Asia Minor and the Black Sea). One might suspect that, in response to warming over the EMED, the anomalous convergence and ascending motion over the EMED triggers a seesaw connection with northward-located regions. This link could stem from the interactions of the anomalous warming and upward velocity anomalies with the seasonally varying descending branch of the Hadley cell over EMED, in result expanding it towards Asia Minor. Testing this hypothesis needs more elaborate analysis and could be the objective of future research.

5. Summary and Discussion

Based on the state-of-the-art future projections (CMIP3 and CMIP5-generation) the Mediterranean has been identified as a climate change hot spot (Giorgi and Lionello 2008), not only due to the sensitivity of its climate to the anthropogenic forcing but also due to the socio-economic vulnerability of the local societies. Yet the projected changes are not fully reflected in the observations for the second half of the 20th century. While the derived anthropogenic fingerprint suggests strong warming and drying during the summer, the observations indicate opposite wetting tendencies for some regions—in the vicinity of Black Sea and off the Balkan coast. This discrepancy may stem from the fact that the Mediterranean climate features abundant cross-scale variations, which at present dominate the anthropogenic signal. But there can be other reasons for this inconsistency, i.e. the deficiencies in models' representation of land-atmospheric feedbacks (as mentioned above) or the deficiencies in capturing impacts of certain teleconnections.

The former has been shown to cause an overestimation of the projected future summer warming and drying in most of CMIP3 and CMIP5 models (Christensen and Boberg, 2012, Christensen and Boberg, 2012, Mueller and Seneviratne, 2014), particularly in the Mediterranean, Central and Southeast Europe (Diffenbaugh et al., 2007, Hirschi et al., 2011, Seneviratne et al., 2006). The coincidence of the amplified drying and warming in these regions has been explained through a ‘‘terrestrial branch’’ of soil moisture–atmosphere interactions (Guo et al. 2006; Dirmeyer 2011, Berg et al. 2015), which cause negative correlations of precipitation and temperature over land in summer. For example, lower precipitation leads to a reduced soil moisture and latent heat flux, thereby increasing sensible heating at the surface and near-surface air temperatures.

The deficiencies in capturing impacts of certain teleconnections has been suggested to incapacitate CMIP3/CMIP5 models in offsetting projected future regional drying, and hence to spuriously exaggerate the regional warming and drying (Blade et al., 2012). Obtaining realistic future projections for this region requires not only refined spatial scales, but also a realistic balance between the contributing impacts of local land-atmosphere feedbacks, large-scale circulation, and teleconnections. In this study, we use the high-resolution CM2.5 climate model integrations to analyze the projected future changes in temperature and precipitation over the Mediterranean and discern between the role of the simulated SNAO teleconnections, and the local impacts of warming land surface and associated land surface –air interactions.

Our analysis demonstrates the high ability of the CM2.5 model in reproducing key large-scale and regional features shaping the complex summer Mediterranean climate thereby highlighting advantages of employed high spatial-resolution. The model accurately captures spatial features and magnitude of the subtropical mid-tropospheric anticyclone extended between the Levant and South Asia, as well as the low-tropospheric zonal pressure gradient between the subtropical North Atlantic anticyclone and the massive Asian monsoon heat low. The pressure gradient, manifested in the Mediterranean as a complex structure of northerly winds, i.e. Etesians, is resolved in the model with great detail including the distinguishable branch over the Aegean Sea and its southward extension toward the Sahel region, as well as the one over the Persian Gulf. The mean precipitation, which features an exceptional spatial complexity in the Mediterranean, is represented with a much higher degree of realism when compared with the low-resolution CM2.1, for example.

Furthermore, we find that CM2.5 faithfully reproduces the most prominent pattern of atmospheric variability over the North Atlantic, i.e. the North Atlantic oscillation, and its impact on the Mediterranean hydroclimate. In the simulations and observations, SNAO emerges as a leading EOF component, explaining ~34% and ~28% of the total variance over the analysis domain, respectively (Folland et al., 2009). Remarkably, the simulated pattern corresponds better to the observed one before the 1970s, rather than for the more recent decades. Moreover, the simulated impact of the SNAO on the Mediterranean hydroclimate is more consistent with the century-long observations (1900-1998, 1900-2007, in Folland et al., 2009), rather than the most recent decades of observations (1950-2010 in Blade et al., 2012). For example, the impact on precipitation and surface temperature derived with the shorter data set is relatively high (with the magnitude of correlations reaches up to 0.5-0.6), but with the significant results confined mostly to the Balkans and Italy. In contrast, the correlations derived for the century-long precipitation record are of lower magnitude (i.e. lower than 0.45), but they are significant over most parts of the Mediterranean, as shown in Folland et al., 2009. The study, mentioned above, explains also that the impact of SNAO is to some extent shaped by its low-frequency variations that may have partly originated from anthropogenic forcing. This forcing contributes to a smaller extent in the observational record before the 1950s and is also not included in the CM2.5 control run. Hence, the apparent ambiguity of the observed SNAO impacts may stem from the varying in time importance of the low-frequency and high-frequency factors which shape the SNAO in the 20th century (as highlighted by Linderholm and Folland, 2017), though this issue still requires further investigation. Further analysis of the

CM2.5 runs shows also that the impacts of the SNAO teleconnection on the Mediterranean precipitation are comparable with those simulated with the previous generation model, such as HADCM3 (Blade et al., 2012). The impacts simulated with CM2.5 are also indistinguishably different from those captured in the GFDL CM2.1 runs (i.e. the low-resolution predecessor of CM2.5), except the region of Asia Minor, where CM2.1 does not capture the significant impact of SNAO.

Moreover, the model skillfully captures the linkage between the low-level northerly flow and the mid- and upper-tropospheric subsidence over the eastern Mediterranean. These two factors have counteracting effects on the regional temperature, hence playing an important role in maintaining the local temperature balance. Therefore, their linkage is the key feature that shapes the summer climate for the eastern Mediterranean. Additionally, the derived correlations between the mid- and upper tropospheric subsidence over the Mediterranean, and the indices of the Indian summer monsoon are consistent with the monsoon-desert mechanism (Rodwell and Hoskins, 1996, and Tyrlis et al., 2013).

Overall, our analysis of the CM2.5 control run confirms the capability of the model to simulate key components of the regional climate, in particular the SNAO teleconnection, and the local linkage between the surface and upper-level dynamics in the Mediterranean summer regime. This allowed us to further investigate the regional future changes through the prism of the evolution of these two factors.

The CM2.5 projections of large-scale climate changes over the Euro-Atlantic region are largely consistent with the CMIP5 ensemble projections. The projected changes in large-scale circulation, i.e. the expansion of the Hadley cell, and the intensification and northward shift of the atmospheric meridional cells, constitute a typical anthropogenic fingerprint of the future changes over the North Atlantic (e.g. Collins et al., 2013, Folland et al., 2009). Consistent with the previous CMIP projections (e.g. Collins et al., 2013), these changes are reflected in the strengthening of the SNAO towards its positive phase (Blade et al. 2012, Folland et al., 2009). For Europe, CM2.5 projects drying over the subtropics (southern Mediterranean) and wetting of the mid-latitudes (northern Europe), which is consistent with the previous generations of the models, and explained with the "wet-get-wetter and dry-get-drier" mechanism (Held and Soden, 2006, Seager et al., 2007).

Nonetheless, the CM2.5 projections show distinguishable differences in the large-scale atmospheric circulation patterns of the future changes and a higher complexity of the derived temperature and precipitation changes over Europe, when compared with the CMIP3 and CMIP5 ensembles. Importantly, CM2.5 simulations imply less radical magnitudes of the warming over most of Europe, fewer regions and smaller magnitudes of drying anomalies, as well as larger areas with wetting anomalies. For example, the CMIP ensembles feature negative SLP tendencies over most of Eurasia, including an intensification of the heat low over the Mediterranean, as contrasted with the CM2.5 projections featuring negative SLP tendencies over the Mediterranean and the positive SLP tendencies over western and central Europe. As a consequence, the former indicates rather a weakening of the atmospheric circulation over the Mediterranean, while the latter indicates a strengthening zonal SLP gradient and hence stronger northerly flow, i.e. Etesian winds, in this region.

Regarding the precipitation changes, CM2.5 simulates a sharp gradient between drying over southwest Europe, including most of the Mediterranean, and wetting over northeast and central Europe, including the Alps and northern parts of Balkans. This feature distinguishes the CM2.5 from the previous CMIP runs, which project mostly a strong drying over whole Europe, except Scandinavia, as depicted for example in the CSIRO-Mk3-6-0 model ensemble (Figure SI5).

Consistent with the previous CMIP ensembles, CM2.5 also projects a strong gradient between warming in southwestern Europe and weaker warming in northeastern Europe. The regions of North Africa and Levant feature the maximum of warming (reaching locally 8°C over summer) in the Mediterranean, while Iberian Peninsula and central parts of the region (i.e. southern France and in Italy) show slightly lower values, i.e. 4-6°C. Nevertheless, the warming projected in CM2.5 is much less radical, when compared to the CMIP3 (Dubrowski et al., 2014) and CMIP5 (Collins et al., 2013) ensembles, as well as the high resolution EURO-CORDEX GCM-RCM RCP8.5 multi-model ensemble (Fussel et al., 2017, Jacob et al., 2014). This discrepancy is distinguishable in particular for the northern Balkans and southeastern Europe, where CM2.5 shows a minimum warming of 0.5-2.5°C, while the other ensembles indicate a warming of 3.5-5.5°C or stronger.

The very intense warming and drying over Europe projected in the CMIP ensembles has been linked to a temperature-dependent warm summertime bias, caused by deficient representations of moisture-temperature feedbacks in most of CMIP3 and CMIP5 models (Christensen and Boberg, 2012, Mueller and Seneviratne, 2014, Boberg and Christensen, 2012). On the other hand, Berg et al. 2016; Milly et al. 2014 demonstrated that the representation of soil moisture and land-atmospheric feedbacks between soil moisture and precipitation in the LM3 model, used in CM2.5, is significantly improved. Moreover, the atmosphere-land interactions have been shown to play an important role in the future summer climate, in particular, over central and southeastern Europe (Seneviratne et al., 2006, Diffenbaugh, 2007, Hirschi et al., 2011). In conclusion, the improvements in the land model incorporated in CM2.5 at its high spatial resolution are responsible for the stark contrast between the CMIP3/CMIP5 and CM2.5 regional projections (i.e. less intense warming and drying over Europe, including the minimum of warming and wetting tendencies in southeastern Europe). These feedbacks should be explored in more detail in future work using targeted experiments like the Global Land-Atmosphere Coupling Experiment (Seneviratne et al., 2013), but lie outside the scope of this paper.

Consistent with previous studies (Blade et al., 2012, Folland et al., 2009), we show that the SNAO may play a role in counterbalancing the projected drying over the Mediterranean. This is due to the projected strengthening of the SNAO towards its positive phase, which is manifest in the positive anomalies of precipitation (wetting) over large parts of the region. Nevertheless, our analysis also shows that a) the representation of the regional SNAO impacts, and b) the projected future evolution of the SNAO is almost the same in CM2.5 and its low-resolution predecessor, i.e. CM2.1 model, or other previous-generation models. Hence the SNAO teleconnection does not seem to be a strong candidate for explaining the differences in the future projections for the summer European climate between CM2.5 and CMIP3/CMIP5 ensembles.

Moreover, the future changes in the eastern Mediterranean climate regime projected in CM2.5 suggest a weakening role of atmospheric dynamics in maintaining the regional hydroclimate and temperature balance. We found a weakening of the linkage between the low-level circulation (e.g. northerly Etesian winds) and the mid- and upper-level subsidence over the eastern Mediterranean, which are responsible for the regional temperature balance. This change, as additional analysis shows, can be explained with the emerging local response of surface circulation, triggered by the warming land. The response (i.e. an anomalous intensification of the heat low over the EMED, Sahara and the Persian trough; anticyclonic anomalies, increasing subsidence and drying over the central Mediterranean; an intensified zonal pressure gradient and Etesian winds) is consistent with the projected in CM2.5 climate change. This supports the concept that warming surface temperature-driven atmospheric responses will become a more prominent factor shaping future Mediterranean climate.

Overall, our analysis indicates very profound climate changes for the Mediterranean region in the summer, although they do not seem to be as radical as projected by the previous generation models. The differences between CM2.5 projections of future changes and those of previous-generation models points to the role of factors such as land surface-atmospheric interactions, in particular over central and southeastern Europe, rather than large-scale atmospheric dynamics and teleconnections. This highlights the importance of the ability of the future-generation models to capture local land-atmospheric interactions.

Code and data availability.
The GFDL CM2.5 model code is publicly available at: https://www.gfdl.noaa.gov/cm2-5-and-flor-quickstart/. Analysis scripts are available on request from the corresponding author.

Author contribution.
All authors contributed to the idea and scope of the paper. M.J.B performed the analyses and wrote the manuscript. S.B.K, L.K., S.R., A.C., C.K.F provided help with data analysis, discussed the results and contributed to the writing of the manuscript. S.B.K provided help with data access and collection.

Competing interests.

The authors declare that they have no conflict of interest.

Acknowledgements

The authors are grateful to Ileana Blade, Fred Kucharski and Eduardo Zorita, Salvatore Pascale and Baoqiang Xiang for helpful comments and discussions.

References:

Alessandri, A., De Felice, M., Zeng, N., Mariotti, A., Pan, Y., Cherchi, A., Lee, J.Y., Wang, B., Ha, K.J., Ruti, P., and Artale, V.: Robust assessment of the expansion and retreat of Mediterranean climate in the 21st century. Sci Rep 4:7211, 2014.

Allan, R. and Folland, C.K.: Atmospheric circulation. 1. Mean sea level pressure and related modes of variability—In: State of the Climate 2017. Bull. Amer. Meteor. Soc., 99, S39-S41, 2018.

Alpert, P., Osetinsky, I., Ziv, B., and Shafir, H.: A new seasons definition based on classified daily synoptic systems: an example for the eastern Mediterranean. Int J Climatol 24:1013–1021, 2004.

Baines, P., and Folland, C.K. : Evidence for a rapid global climate shift across the late 1960s. J. Climate, 20, 2721-2744, 2007.

Barcikowska, M., Knutson, T. and Zhang, R.: Observed and simulated fingerprints of multidecadal climate variability, and their contributions to periods of global SST stagnation. Journal of Climate, 30(2), 2017.

Barcikowska, M., Kapnick, S.B., and Feser, F.: Impact of large-scale circulation changes in the North Atlantic sector on the current and future Mediterranean winter hydroclimate. Climate Dynamics, 2017b.

Barnston, A.G., Livezey, R.E.: Classification, seasonality and persistence of low-frequency atmospheric circulation patterns. Mon Wea Rev 115:1083–1126, 1987.

Berg, A., B.R. Lintner, K. Findell, S.I. Seneviratne, B. van den Hurk, A. Ducharne, F. Chéruy, S. Hagemann, D.M. Lawrence, S. Malyshev, A. Meier, and Gentine, P.: Interannual Coupling between Summertime Surface Temperature and Precipitation over Land: Processes and Implications for Climate Change. J. Climate, 28, 1308–1328, 2015.

Berg, A., Findell, K., Lintner, B., Giannini, A., Seneviratne, S. I., Van den Hurk, B., Ruth Lorenz, Andy Pitman, Stefan Hagemann, Arndt Meier, Frédérique Cheruy, Agnès Ducharne, Sergey Malyshev, and Milly, P. C. D.: Land–atmosphere feedbacks amplify aridity increase over land under global warming. Nature Climate Change, 6(9), 869, 2016.

Berg, A. et al.: Interannual coupling between summertime surface temperature and precipitation over land: processes and implications for climate change. J. Clim. 28, 1308 132, 2015.

Blade, I., Liebmann, B., Fortuny, D., and van Oldenborgh, G.J.: Observed and simulated impacts of the summer NAO in Europe: implications for projected drying in the Mediterranean region. Clim Dyn 39:709–727, 2012.

Blade, I., D. Fortuny, van Oldenborgh, G.J., and Liebmann, B.: The summer North Atlantic Oscillation in CMIP3 models and related uncertainties in projected summer drying in Europe, J. Geophys. Res., 117, D16104, 2012b.

Bitan, A. and Saaroni, H.: The horizontal and vertical extension of the Persian Gulf pressure trough. Int J Climatol 12:733–747, 1992.

Booth, B.B.B., Dunstone, N.J., Halloran, P.R., Andrews, T., and Bellouin, N.: Aerosols implicated as a prime driver of twentieth-century North Atlantic climate variability, Nature, 484, 228–232, 2012.

Cassou, C., L. Terray, J. W. Hurrell, and Deser, C.: North Atlantic winter climate regimes: Spatial asymmetry, stationarity with time, and oceanic forcing. J. Climate, 17, 1055–1068, 2004.

Cassou, C., L. Terray, and Phillips, A.S.: Tropical Atlantic influence on European heat waves. J. Climate, 18, 2805–2811, 2005.

Cherchi, A., Annamalai, H., Masina, S., and Navarra, A.: South Asian summer monsoon and eastern Mediterranean climate: the monsoon- desert mechanism in CMIP5 simulations. J Clim 27: 6877– 6903, 2014.

Cherchi, A., Annamalai, H., and Masina, S.: Clim Dyn, 47: 2361. https://doi.org/10.1007/s00382-015-2968-4, 2016.

Cheruy, F., J. L. Dufresne, F. Hourdin, and Ducharne, A.: Role of clouds and land -atmosphere coupling in midlatitude continental summer warm biases and climate change amplification in CMIP5 simulations, Geophys. Res. Lett., 41, 6493–6500, doi:10.1002/2014GL061145, 2014.

Christensen, J. H., and Boberg, F.: Temperature dependent climate projection deficiencies in CMIP5 models, Geophys. Res. Lett., 39, L24705, doi:10.1029/2012GL053650, 2012.

Chronis, T., Raitsos, D.E., Kassis, D., and Sarantopoulos, A.: The summer North Atlantic oscillation influence on the Eastern Mediterranean. J Clim 24:5584–5596, 2011.

Collins, M., R. Knutti, J. Arblaster, J.-L. Dufresne, T. Fichefet, P. Friedlingstein, X. Gao, W.J. Gutowski, T. Johns, G. Krinner, M. Shongwe, C. Tebaldi, A.J. Weaver and M. Wehner, 2013: Long-term Climate Change: Projections, Commitments and Irreversibility. In: Climate Change 2013: The Physical Science Basis. Contribution of Working Group I to the Fifth Assessment Report of the Intergovernmental Panel on Climate Change [Stocker, T.F., D. Qin, G.-K. Plattner, M. Tignor, S.K. Allen, J. Boschung, A. Nauels, Y. Xia, V. Bex and P.M. Midgley (eds.)]. Cambridge University Press, Cambridge, United Kingdom and New York, NY, USA, 2013.

Compo, G.P., J.S. Whitaker, and Sardeshmukh, P.D.: Feasibility of a 100 year reanalysis using only surface pressure data. Bull. Amer. Met. Soc., 87, 175-190, http://dx.doi.org/10.1175/BAMS-87-2-175, 2006.

Compo, G.P., J. S. Whitaker, P. D. Sardeshmukh, N. Matsui, R. J. Allan, X. Yin, B. E. Gleason Jr., R. S. Vose, G. Rutledge, P. Bessemoulin, S. Brönnimann, M. Brunet, R. I. Crouthamel, A. N. Grant, P. Y. Groisman, P. D. Jones, M. C. Kruk, A. C. Kruger, G. J. Marshall, M. Maugeri, H. Y. Mok, Ø. Nordli, T. F. Ross, R. M. Trigo, X. L. Wang, S. D. Woodruff, Worley, S.J.: The twentieth century reanalysis project. Q. J. R. Meteorol. Soc. 137, 1–28, 2011.

Cornes, R., G. van der Schrier, E.J.M. van den Besselaar, and Jones, P. D.: An Ensemble Version of the E-OBS Temperature and Precipitation Datasets, J. Geophys. Res. Atmos., 123, 2018.

Delworth, T.L., A.J. Broccoli, A. Rosati, R.J. Stouffer, V. Balaji, J.A. Beesley, W.F. Cooke, K.W. Dixon, J. Dunne, K.A. Dunne, J.W. Durachta, K.L. Findell, P. Ginoux, A. Gnanadesikan, C.T. Gordon, S.M. Griffies, R. Gudgel, M.J. Harrison, I.M. Held, R.S. Hemler, L.W. Horowitz, S.A. Klein, T.R. Knutson, P.J. Kushner, A.R. Langenhorst, H. Lee, S. Lin, J. Lu, S.L. Malyshev, P.C. Milly, V. Ramaswamy, J. Russell, M.D. Schwarzkopf, E. Shevliakova, J.J. Sirutis, M.J. Spelman, W.F. Stern, M. Winton, A.T. Wittenberg, B. Wyman, F. Zeng, and R. Zhang, GFDL's CM2 Global Coupled Climate Models. Part I: Formulation and Simulation Characteristics. J. Climate, 19, 643–674, 2006.

Delworth, T.L., A. Rosati, W. Anderson, A.J. Adcroft, V. Balaji, R. Benson, K. Dixon, S.M. Griffies, H. Lee, R.C. Pacanowski, G.A. Vecchi, A.T. Wittenberg, F. Zeng, and Zhang, R.: Simulated Climate and Climate Change in the GFDL CM2.5 High-Resolution Coupled Climate Model. J. Climate, 25, 2755–2781, 2012.

Delworth, T. and Mann, M.: Observed and simulated multidecadal variability in the Northern Hemisphere Climate Dynamics, 16: 661, 2000.

Diffenbaugh, N. S., J. S. Pal, F. Giorgi, and Gao, X.: Heat stress intensification in the Mediterranean climate change hotspot, Geophys. Res. Lett., 34, L11706, doi:10.1029/2007GL030000, 2007.

Dirmeyer, P. A.: The terrestrial segment of soil moisture– climate coupling. Geophys. Res. Lett., 38, L16702, doi:10.1029/2011GL048268, 2011.

Enfield, D. B., Mestas‐Nunez, A.M., Trimble, P. J.: The Atlantic multidecadal oscillation and its relation to rainfall and river flows in the continental U.S., Geophys. Res. Lett., 28, 2077–2080, 2001.

Fontaine, B., Roucou, P., Gaetani, M. and Marteau, R.: Recent changes in precipitation, ITCZ convection and northern tropical circulation over North Africa (1979–2007). Int. J. Climatol., 31: 633-648, 2011.

Giorgi, F.: Climate change hot‐spots, Geophys. Res. Lett., 33, L08707, 2006.

Giorgi, F. and Lionello, P.: Climate change projections for the Mediterranean region. Glob Planet Change 63:90–104, 2008.

Feng, S., Hu, Q., Huang, W., Ho, C.-H., Li, R. and Tang, Z.: Projected climate regime shift under future global warming from multi-model, multi-scenario CMIP5 simulations. Global Planet. Change 112, 41–52, 2014.

Füssel, H.M., André Jol, Andreas Marx, et al. edited by Hans-Martin Füssel, André Jol, Andreas Marx, Mikael Hildén: Climate change, impacts and vulnerability in Europe 2016 - An indicator-based report Vol. 1, 2017.

Folland, C.K., Knight, J., Linderholm, H.W., Fereday, D., Ineson, S., Hurrell, J.W.: The summer North Atlantic Oscillation: past, present, and future. J Climate 22:1082–1103, 2009.

Guo, Z., et al.: GLACE: The Global Land– Atmosphere Coupling Experiment. Part II: Analysis. J. Hydrometeor. 7, 611–625, doi:10.1175/JHM511.1., 2006

Hanf, F., Körper, J., Spangehl, T. and Cubasch, U.: Shifts of climate zones in multi-model climate change experiments using the Köppen climate classification. Meteorol. Z. 21, 111–123, 2012.

Hoskins, B.J.,: On the existence and strength of the summer subtropical anticyclones —Bernhard Haurwitz memorial. Bull Am Meteorol Soc 77:1287–1292, 1996.

HMSO: Weather in the Mediterranean I: general meteorology, 2nd edn. Her Majesty Stationery Office, London, 362, 1962.

Hurrell, J. W.: Decadal trends in the North Atlantic Oscillation: regional temperatures and precipitation. Science 269: 676–679, 1995.

Hurrell, J.W., Deser, C.: North Atlantic climate variability: the role of the North Atlantic Oscillation. J Mar Syst 78(1): 28–41, 2009.

Hurrell, J.W., and Folland, C. K.: A change in the summer circulation over the North Atlantic. CLIVAR Exchanges, No. 25, International CLIVAR Project Office, Southampton, United Kingdom, 52–54, 2002.

Hurrell, J.W., Kushnir, Y., Ottersen, G., Visbeck, M.: An overview of the North Atlantic Oscillation. The North Atlantic Oscillation: climatic significance and environmental impact. Geophys Monogr. Am Geophys Union 134:1–35, 2003.

Hurrell, J. W., and H. van Loon: Decadal variations in climate associated with the North Atlantic Oscillation. Climatic Change, 36, 301–326, 1997.

Jacob, D., Petersen, J., Eggert, B., Alias, A., Christensen, O. B., Bouwer, L. M., Braun, A., Colette, A., Déqué, M., Georgievski, G., Georgopoulou, E., Gobiet, A., Menut, L., Nikulin, G., Haensler, A., Hempelmann, N., Jones, C., Keuler, K., Kovats, S.: 'EURO-CORDEX: New high-resolution climate change projections for European impact research', Regional Environmental Change 14(2), 563–578, 2014.

Kalnay et al.,: The NCEP/NCAR 40-year reanalysis project, Bull. Amer. Meteor. Soc., 77, 437-470, 1996.

Kanamitsu, M., W. Ebisuzaki, J. Woollen, S. Yang, J.J. Hnilo, M. Fiorino, and Potter, G. L.: NCEP–DOE AMIP-II Reanalysis (R-2). Bull. Amer. Meteor. Soc., 83, 1631–1644, 2002.

Kapnick, S. B., Delworth, T. L., Ashfaq, M., Malyshev, S., & Milly, P. C.: Snowfall less sensitive to warming in Karakoram than in Himalayas due to a unique seasonal cycle. *Nature Geo.*, *7*(11), 834, 2014.

Kelley, C., Ting, M., Seager, R., Kushnir, Y.: Mediterranean precipitation climatology, seasonal cycle, and trend as simulated by CMIP5. Geophys Res Lett 39:L21703, 2012.

Krichak, S.O., Kishcha, P., Alpert, P.: Decadal trends of main Eurasian oscillations and the Mediterranean precipitation, Teor. Appl. Climatol., 72: 29-220, 2002.

Knight, J. R., R. J. Allan, C. K. Folland, M. Vellinga, and Mann, M.E.: A signature of persistent natural thermohaline circulation cycles in observed climate. Geophys. Res. Lett., 32, L20708, 2005.

Knight, J. R., R., C. K. Folland, and Scaife, A.A.: Climatic impacts of the Atlantic multidecadal oscillation. Geophys. Res. Lett., 33, L17706, 2006.

Knutti, R., Masson, D. & Gettelman, A. Climate model genealogy: Generation CMIP5 and how we got there. Geophys. Res. Lett. 40, 1194–1199, 2013.

Kotlarski, S., Keuler, K., Christensen, O. B., Colette, A., Déqué, M., Gobiet, A., Goergen, K., Jacob, D., Lüthi, D., van Meijgaard, E., Nikulin, G., Schär, C., Teichmann, C., Vautard, R., Warrach-Sagi, K., and Wulfmeyer, V.: Regional climate modeling on European scales: a joint standard evaluation of the EURO-CORDEX RCM ensemble, Geosci. Model Dev., 7, 1297–1333, https://doi.org/10.5194/gmd-7-1297-2014, 2014.

Legates, D. R., and Willmott, C. J.: Mean seasonal and spatial variability in gauge-corrected, global precipitation. Int. J. Climatol.,10, 111–127, 1990.

Lelieveld, J., Berresheim, H., Borrmann, S.: Global air pollution crossroads over the Mediterranean. Science 298: 794–799, 2002.

Lelieveld, J., Hadjinicolaou, P., Kostopoulou, E., Chenoweth, J., Giannakopoulos, C., Hannides, C., Lange, M.A., El Maayar, M., Tanarthe, M., Tyrlis, E., and Xoplaki, E.: Climate change and impacts in the eastern Mediterranean and the Middle East. Clim Chang 114:667–687, 2012.

Lin, H.: Global extratropical response to diabatic heating variability of the Asian summer monsoon. J Atmos Sci 66: 2697–2713, 2009.

Lin, H., Derome, J., Brunet, G.: The nonlinear transient atmospheric response to tropical forcing. J Clim 20:5642–5665, 2007.

Linderholm, H.W. and C K. Folland,: Summer North Atlantic Oscillation (SNAO) variability on interannual to palaeoclimate time scales. CLIVAR Exchanges 72, 57-60 and Past Global Changes Magazine, 25, No. 1., 2017.

Linderholm, H.W., Folland, C.K. and Walther, A.: A multicentury perspective on the summer North Atlantic Oscillation (SNAO) and drought in the eastern Atlantic Region. J. Quaternary Science, 24, 415-425, 2009.

Lundquist, J., Hughes, M., Gutmann, E. and Kapnick, S.: Our skill in modeling mountain rain and snow is bypassing the skill of our observational networks. *Bulletin of the American Meteorological Society*, doi: 10.1175/BAMS-D-19-0001.1, 2019.

Maheras, P.: Le problem des Etesiens. Mediterranee, N40, 57-66, 1980.

Mann, M. E., and Emanuel, K.A.: Atlantic hurricane trends linked to climate change, Eos Trans. AGU, 87(24), 233–241, doi: 10.1029/2006EO240001, 2006.

Mariotti, A., Dell'Aquila, A.: Decadal climate variability in the Mediterranean region: roles of large-scale forcings and regional processes. Clim Dyn 38:1129–1145, 2012.

Mariotti, A., Pan, Y., Zeng, N., and Alessandri, A.: Long-term climate change in the Mediterranean region in the midst of decadal variability. Clim Dyn 44:1437–1456, 2015.

Mariotti, A., Struglia, M.V., Zeng, N., and Lau, K.M.: The hydrological cycle in the Mediterranean region and implications for the water budget of the Mediterranean Sea. J Clim 15:1674–1690, 2002.

Meehl, G., A. et al. Global climate projections. In: Solomon S et al. (eds) Climate change 2007: The Physical Science Basis. Cambridge University Press, Cambridge,747–845, 2007.

Meinshausen, M. and Smith,J. S and Calvin, K.V. and Daniel, J., and Kainuma, M., and Lamarque, J.-F. and Matsumoto, K., and A Montzka, S., C B Raper, S., and Riahi, K. and Thomson, A.M. and Velders, Guus J. M., and Vuuren, D: The RCP greenhouse gas concentrations and their extensions from 1765 to 2300. Climatic Change, 2011.

Metaxas D.A: The interannual variability of the Etesian frequency as a response of atmospheric circulation anomalies. Bulletin of the Hellenic Meteorological Society 2(5): 30–40, 1977.

Milly, P. C. D.,Shmakin, A.B.: Global modeling of land water and energy balances. Part I: The Land Dynamics (LaD) model. J. Hydrometeor., 3, 283–299, 2002.

Milly, P.C., S.L. Malyshev, E. Shevliakova, K.A. Dunne, K.L. Findell, T. Gleeson, Z. Liang, P. Phillipps, R.J. Stouffer, and Swenson, S.: An Enhanced Model of Land Water and Energy for Global Hydrologic and Earth-System Studies. J. Hydrometeor., 15, 1739–1761, 2014.

Mueller, B., and Seneviratne, S.I.: Systematic land climate and evapotranspiration biases in CMIP5 simulations, Geophys. Res. Lett., 41, 128–134, 2014.

Mueller, B., and Seneviratne, S.I.: Hot days induced by precipitation deficits at the global scale, Proc. Natl. Acad. Sci. U. S. A., 109, 12,398–12,403, doi:10.1073/pnas.1204330109, 2012.

Pascale, S., Bordoni, S., Kapnick, S. B., and coauthors: The impact of horizontal resolution on North American monsoon Gulf of California moisture surges in a suite of coupled global climate models. *Journal of Climate*, *29*(21), 7911-7936, 2016.

Prezerakos, N.G.: Does the extension of the Azores anticyclone towards the Balkans really exist. Archive fur Meteorologie, Geophysile und Bioklimatologie, Serie A: Meteorologie und Geophysik 33: 217–227, 1984.

Poli, P., H. Hersbach, P. Berrisford, and coauthors: ERA-20C Deterministic. ERA Report Series Number 20, 2015.

Riahi, K., Rao, S., Krey, V. et al. Climatic Change, 109: 33, 2011.

Raicich, F., Pinardi, N., and Navarra, A.: Teleconnections between Indian monsoon and Sahel rainfall and the Mediterranean. Int J Climatol 23:173–186, 2003.

Rizou, D., Flocas, H.A., Athanasiadis, P., and Bartzokas, A.: Relationship between the Indian summer monsoon and the large-scale circulation variability over the Mediterranean, Atmospheric Research, Volume 152, 159-169, 2015.

Reddaway, J.M. and Bigg, G.R.: Climatic change over the Mediterranean and links to the more general atmospheric circulation. Int J Climatol 16:651–661, 1996.

Rodwell, M.J., and Hoskins, B.J.: Monsoons and the dynamics of deserts. Q J R Meteorol Soc 122:1385–1404, 1996.

Rodwell, M.J., and Hoskins, B.J.: Subtropical anticyclones and summer monsoons. J Clim 14:3192–3211, 2001.

Rotstayn, L., and U. Lohman: Tropical rainfall trends and the indirect aerosol effect. J. Climate, 15, 2103–2116, 2002.

Rowell, D. P.: The Impact of Mediterranean SSTs on the Sahelian Rainfall Season. J. Climate, 16, 849–862, 2003.

Rowell, D.P. and Jones, R. G.: Causes and uncertainty of future summer drying over Europe. Climate Dynamics, 27: 281-299, 2006.

Saaroni, H. and Ziv, B.: Summer rain episodes in a Mediterranean climate, the case of Israel: climatological-dynamical analysis. Int J Climatol 20:191–209, 2000.

Saaroni, H., Ziv, B., Osetinsky, I., and Alpert, P.: Factors governing the interannual variation and the long-term trend of the 850 hPa temperature over Israel. Q J R Meteorol Soc 136:305–318, 2010.

Sacks, W.J., Cook, B.I., Buenning, N., Levis, S. and Helkowski, J.H.: Effects of global irrigation on the near-surface climate. *Climate Dynamics*, *33*(2-3), 159-175, 2009.

Scaife, A., Folland, C.K., Alexander, L.V. Moberg, A., Brown, S. and Knight, J. R.: European climate extremes and the North Atlantic Oscillation. J. Climate, 21, 72-83, 2008.

Seneviratne, S. I., D. Lüthi, M. Litschi, and Schär, C.: Land atmosphere coupling and climate change in Europe, Nature, 443 (7108), 205–209, 2006.

Seneviratne, S. I., et al.: Changes in climate extremes and their impacts on the natural physical environment, in Managing the Risks of Extreme Events and Disasters to Advance Climate Change Adaptation. A Special Report of Working Groups I and II of the Intergovernmental Panel on Climate Change (IPCC), edited by C. B. Field et al., pp. 109–230, Cambridge Univ. Press, Cambridge, U. K, 2012.

Seneviratne, S. I. et al: Impact of soil moisture-climate feedbacks on CMIP5 projections: first results from the GLACE-CMIP5 experiment. Geophys. Res. Lett. 40, 5212-5217, 2013.

Sutton, R. T., and Hodson, D.L.R.: Atlantic Ocean forcing of the North American and European summer climate. Science, 309, 115–118, 2005.

Trenberth K.E., and Paolino D.A.Jr: The Northern Hemisphere sea level pressure data set: trends, errors and discontinuities. Mon Wea Rev, 108:855–872, 1980.

Tyrlis, E., Lelieveld, J., and Steil, B.: The summer circulation over the Eastern Mediterranean and the Middle East: influence of the South Asian monsoon. Clim Dyn 40:1103–1123, 2013.

Willmott, C. J. and Matsuura, K.: Terrestrial Air Temperature and Precipitation: Monthly and Annual Time Series (1950 - 1999), 2001.

Zecchetto, S. and de Biasio, F.: Sea surface winds over the Mediterranean basin from satellite data (2000-04): meso- and local-scale features on annual and seasonal time scales. J Appl Meteorol Climatol 46: 814–827, 2007.

Ziv, B., Saaroni, H., and Alpert, P.: The factors governing the summer regime of the eastern Mediterranean. Int J Climatol 24:1859–1871, 2004.

Table1 Abbreviation names for the CM2.5 experiments

NAME of the experiment	**Ensemble size**	**Number of years total**	**Historical period [yrs]**
CTRL	1	1000 yrs	-
HIST	5	145	1861-2005
PROJ	5	95	2006-2100

FIGURES

Figure 1. Seasonal (JJA) time-mean sea level pressure (hPa) and wind vector at 850hPa (m/s) in a) NCEP-DOE2, b) CM2.5. Seasonal (July) time-mean vertical velocities at 500hPa (Pa/s, downward motion denoted with positive values) and wind vectors at 200hPa (Pa/s, downward motion denoted with positive values), estimated for c) NCEP-DOE2, and d) CM2.5 CTRL. Observational data is used for 1979-2017, control simulations data is used for years 101–1000. All data sets are interpolated to the 2.5° horizontal grid.

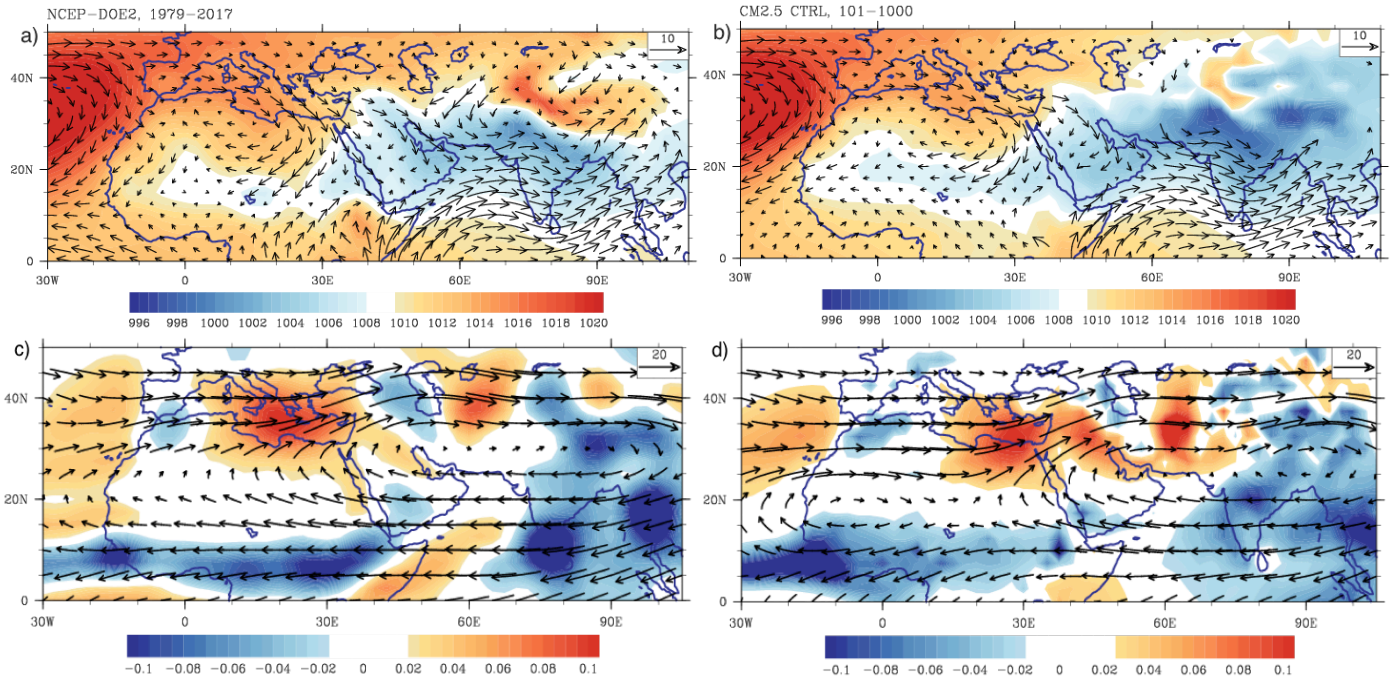

Figure 2. Height (pressure)-longitude cross-section of vertical velocity (Pa/s, shaded contours, downward motion denoted with positive values) and vector of zonal wind (m/s) and vertical velocity (converted to m/s and scaled with a factor of 1000) in July. Figure shows time-mean values in July a) derived for the period 1979-2017 in NCEP-DOE2, b) derived from 101-1000 years of CTRL run in CM2.5; and c) projected future changes in the period 2061-2099 in PROJ ensemble mean, compared with the baseline period 1961-1999 in the HIST ensemble mean. All fields are shown on the 2.5°x2.5° horizontal grid and at the original vertical levels, common for CM2.5 and NCEP-DOE2.

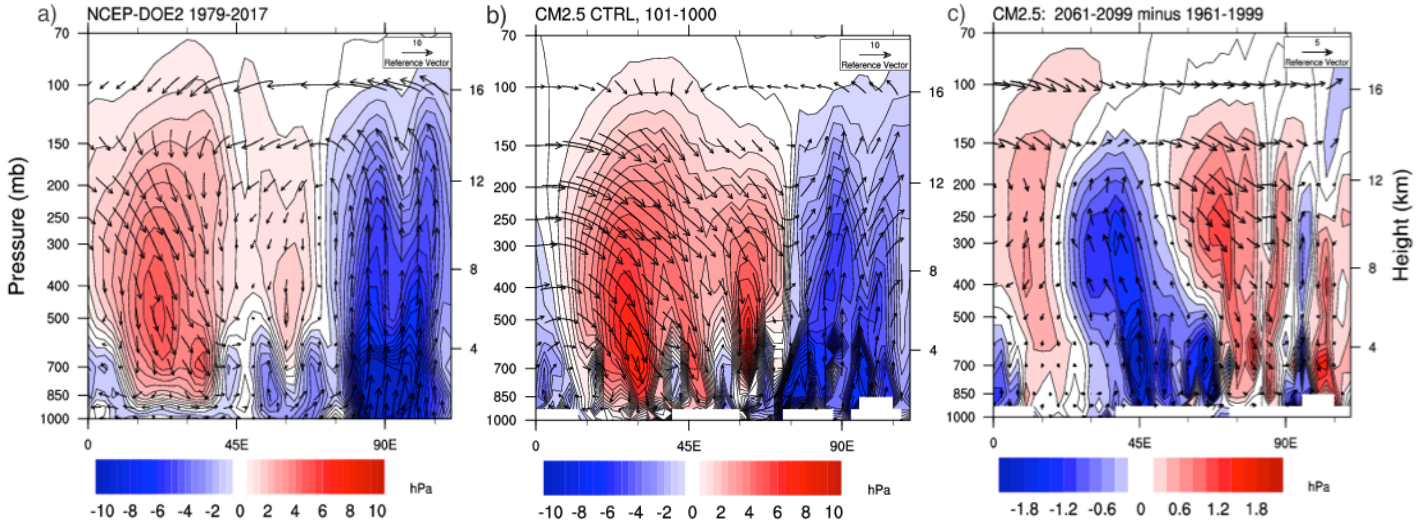

Figure 3. Seasonal (JJA) mean precipitation (mm/day) for a) EOBS observations, b) University of Delaware Climatology, b) CM2.1, c) CM2.5. The time-mean of seasonal data from years 101–1000 of the control simulations are used, and years 1980-2015 of the observed data sets. Both observational data sets are shown at 0.5° lat x lon resolution. Regions with missing data are left blank.

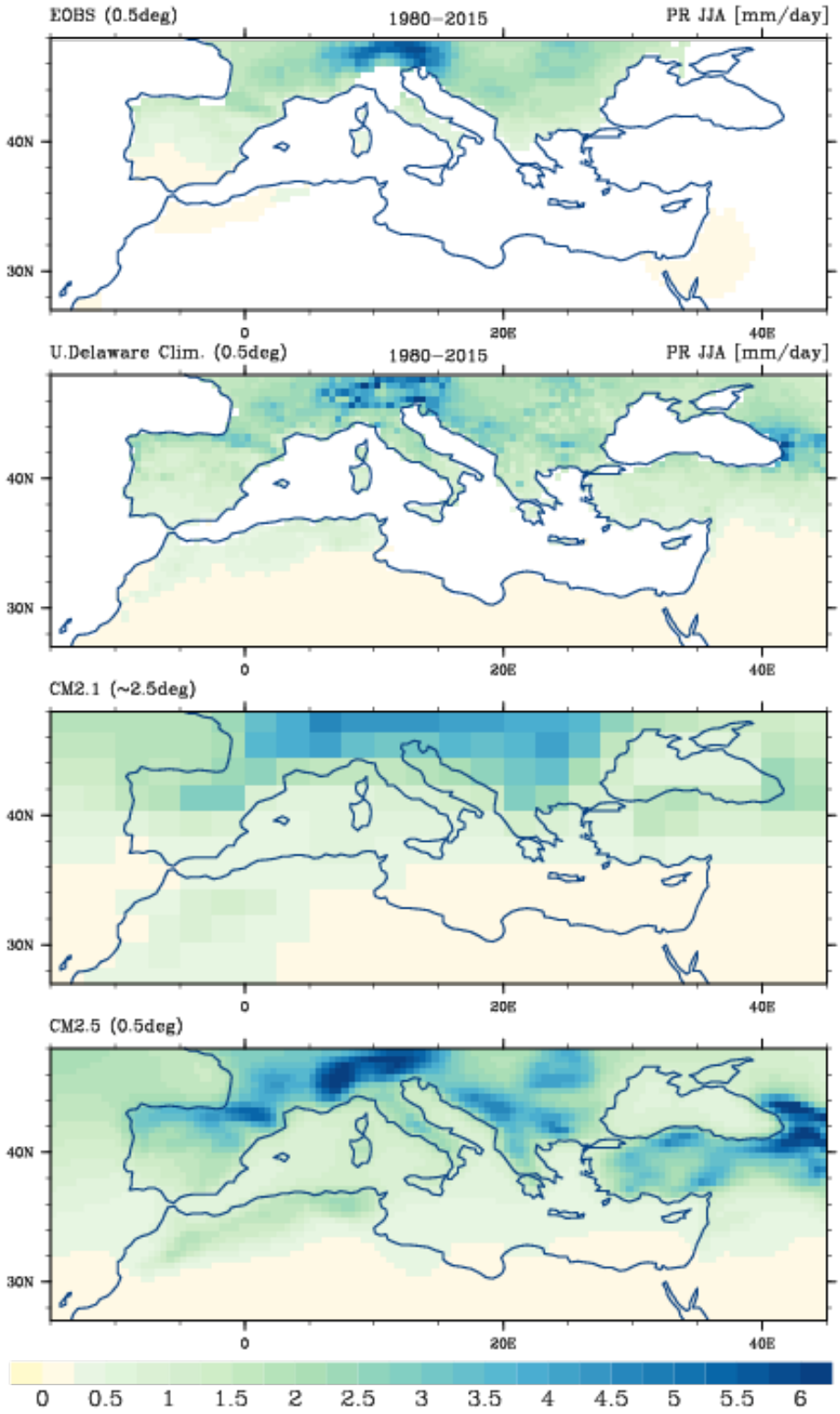

Figure 4. Correlation between principal component time series of the SNAO SLP in JA and a) sea level pressure b) temperature at 2m (shaded) and geopotential height at 850hPa (contours), c) precipitation. All derived from the CTRL run. Contours in a) and c) are shown for 0.25 and 0.5 correlations. Correlations are shown only when significant at 1% level.

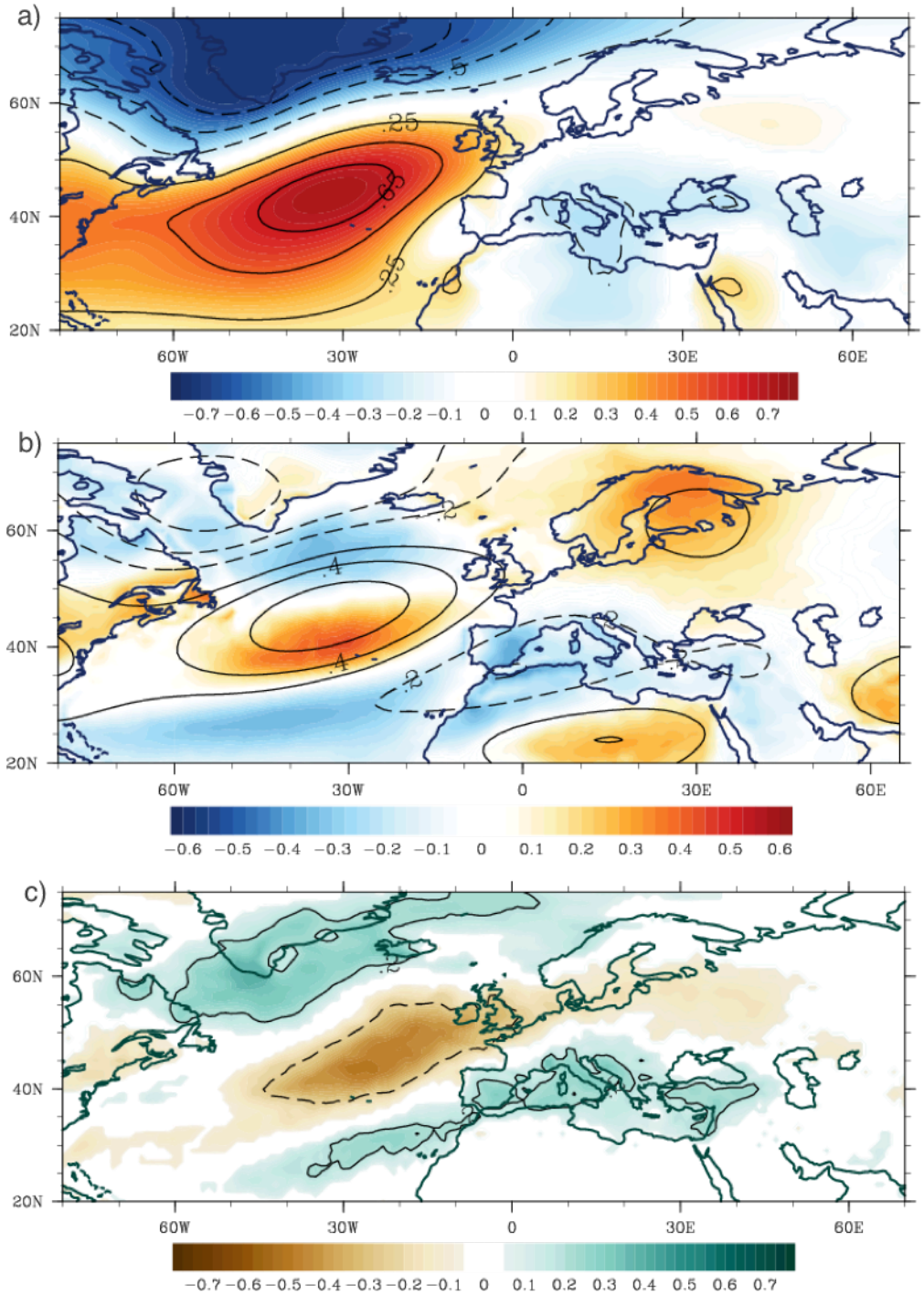

Figure 5. Spatial pattern of the SNAO (EOF), derived from the 20CR reanalysis (left), and from the first CM2.5 HIST run (right), shown as correlations between the first principal component time series and SLP in July-August. The pattern is derived from periods a)-b) 1870-1920, c)-d) 1900-1950, e)-f) 1940-1990, g)-h) 1960-2010. Please note that the sign of each derived EOF is arbitrary. The analysis took into account that fact and unified the sign, showing the SNAO at its positive phase.

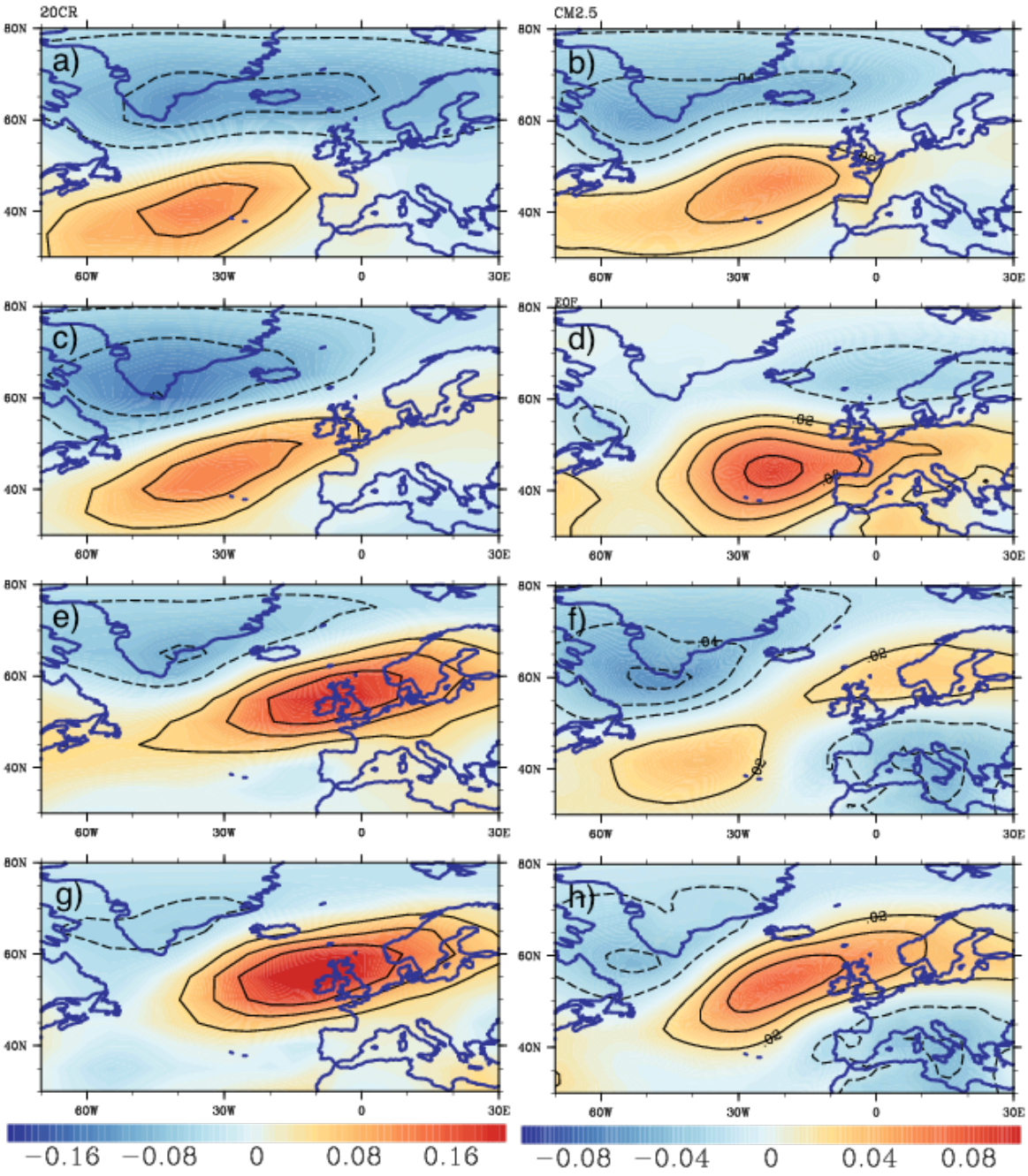

Figure 6. a) First EOF of the vertical velocity at 500 hPa (EOF1 omega, shaded) and at 300hPa (contours), derived for each level separately and from the monthly mean of July in the CTRL run. The time series of EOF1 omega at 500 hpa are correlated with b) geopotential height (shaded), u, v components (shown as vector) at 850hPa, c) meridional wind at 850hPa, e) outgoing long wave radiation (shaded), omega at 500 hPa (contours: -0.2, 0.2, 0.4), f) precipitation. d) Correlations derived between the observed (NCEP) omega 500hPa over the eastern Mediterranean region (32°-34°N, 25°-30°E) and the meridional wind at 850hPa. Correlations shown for b), c), e), f) at the 1%, and for d) the 10% significance level.

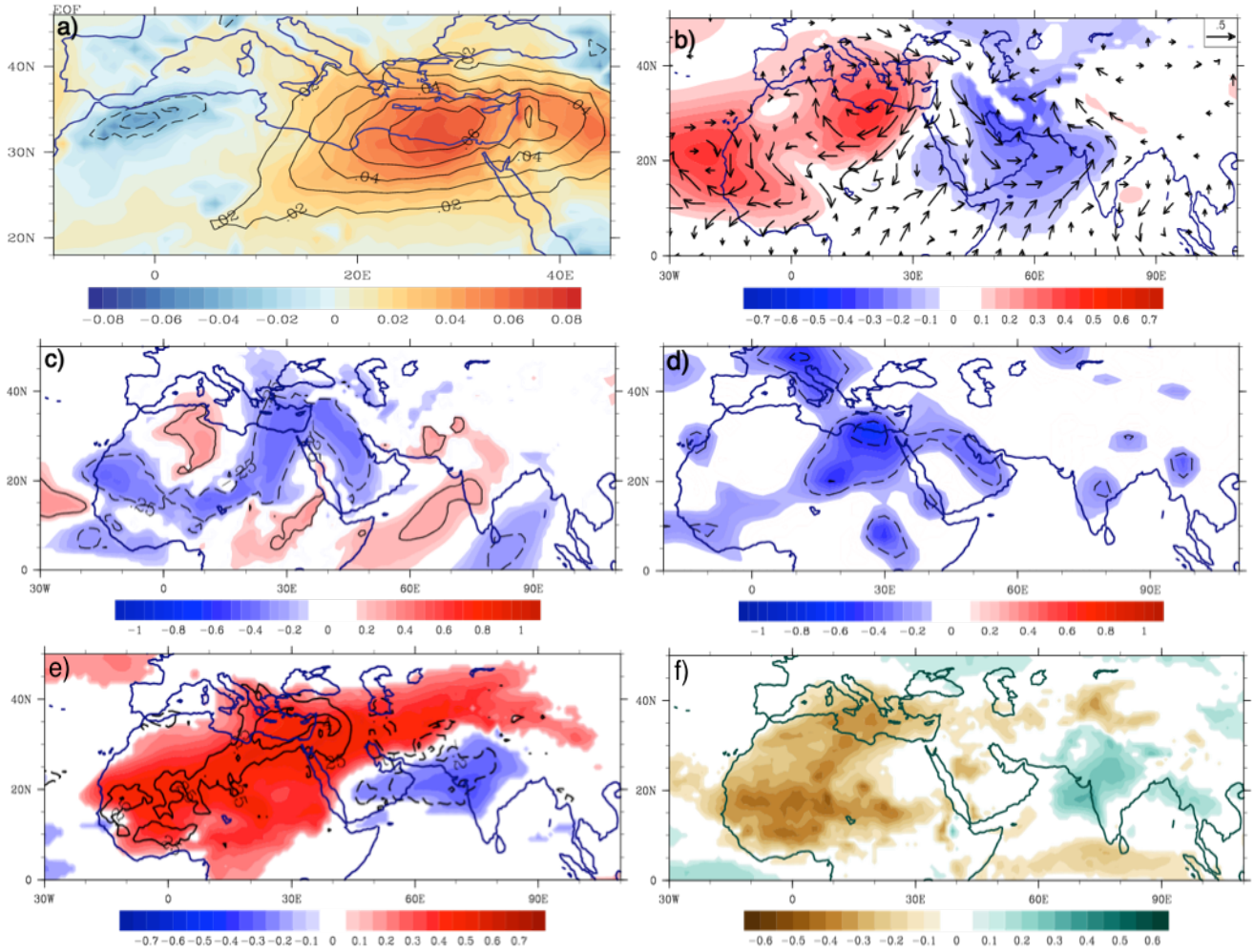

Figure 7. Projected future changes for the summer (JJA) a) sea level pressure (hPa, shaded) and u,v wind components at 850hPa (m/s, vector), b) surface temperature (°C), c) total precipitation rate [mm/day], over the period 2061-2099 compared with the baseline period 1961-1999. Changes are derived at the original horizontal resolution.

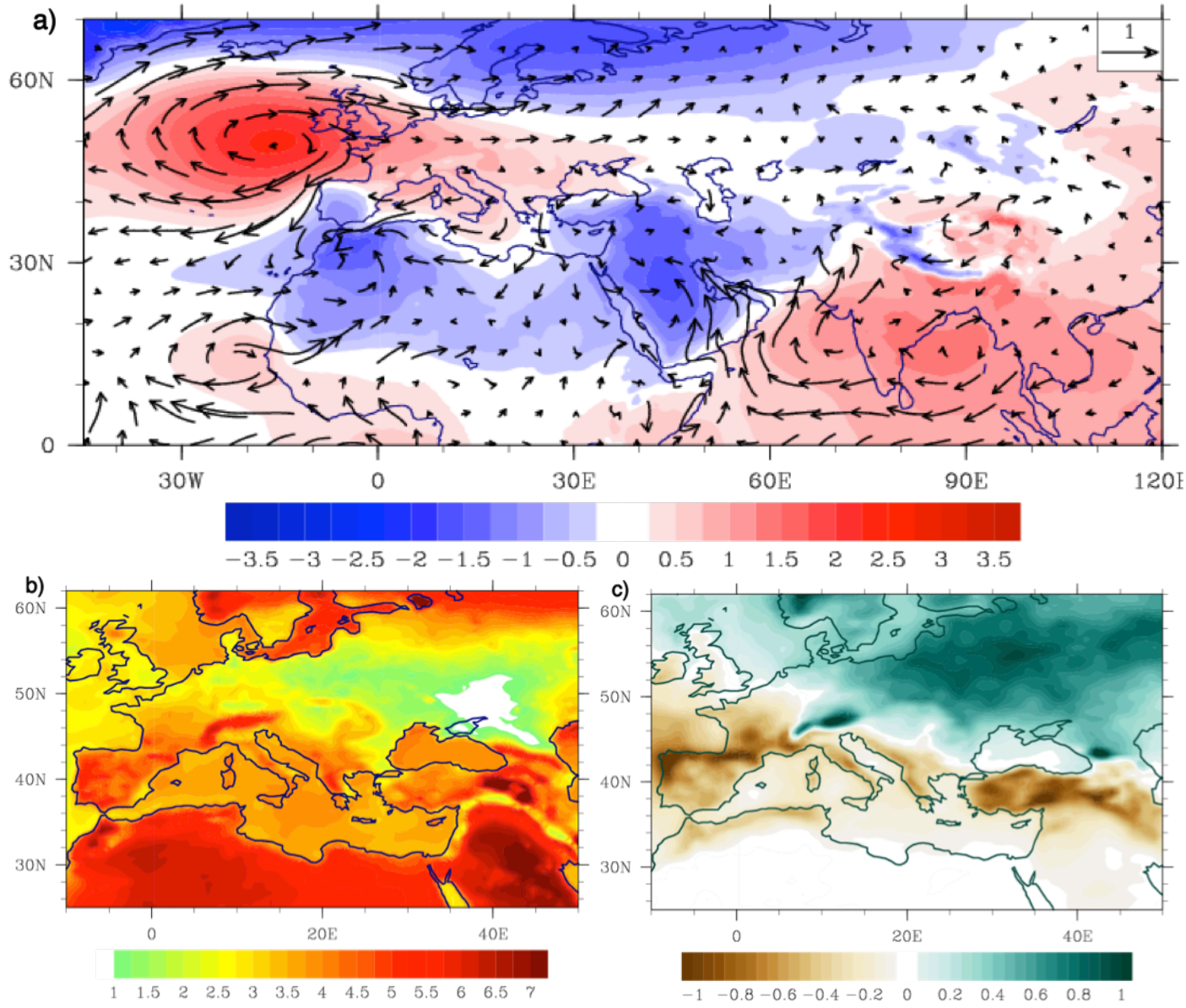

Figure 8. (a, b) Correlations (shaded) between the SNAO time series and precipitation in1900-1950 (a) HIST runs), and 2050-2100 (b) PROJ runs). Contours denote 0.25 and 0.5. c) Evolution of SNAO SLP time series in 1850-2100 period for each run (blue) and the ensemble mean (red). The vertical line divides the HIST and PROJ time series. (d, e) Projected future changes in the summer precipitation (mm/day) (as in Fig 8c, except that estimated at 1° horizontal resolution), d) including SNAO impact and e) with the impact of the future SNAO removed (shaded). Contours in e) denote regions where the drying is stronger by 0.15 mm/day, compared to d). The impact of SNAO is estimated based on the linear regression between the detrended time series of SNAO and precipitation.

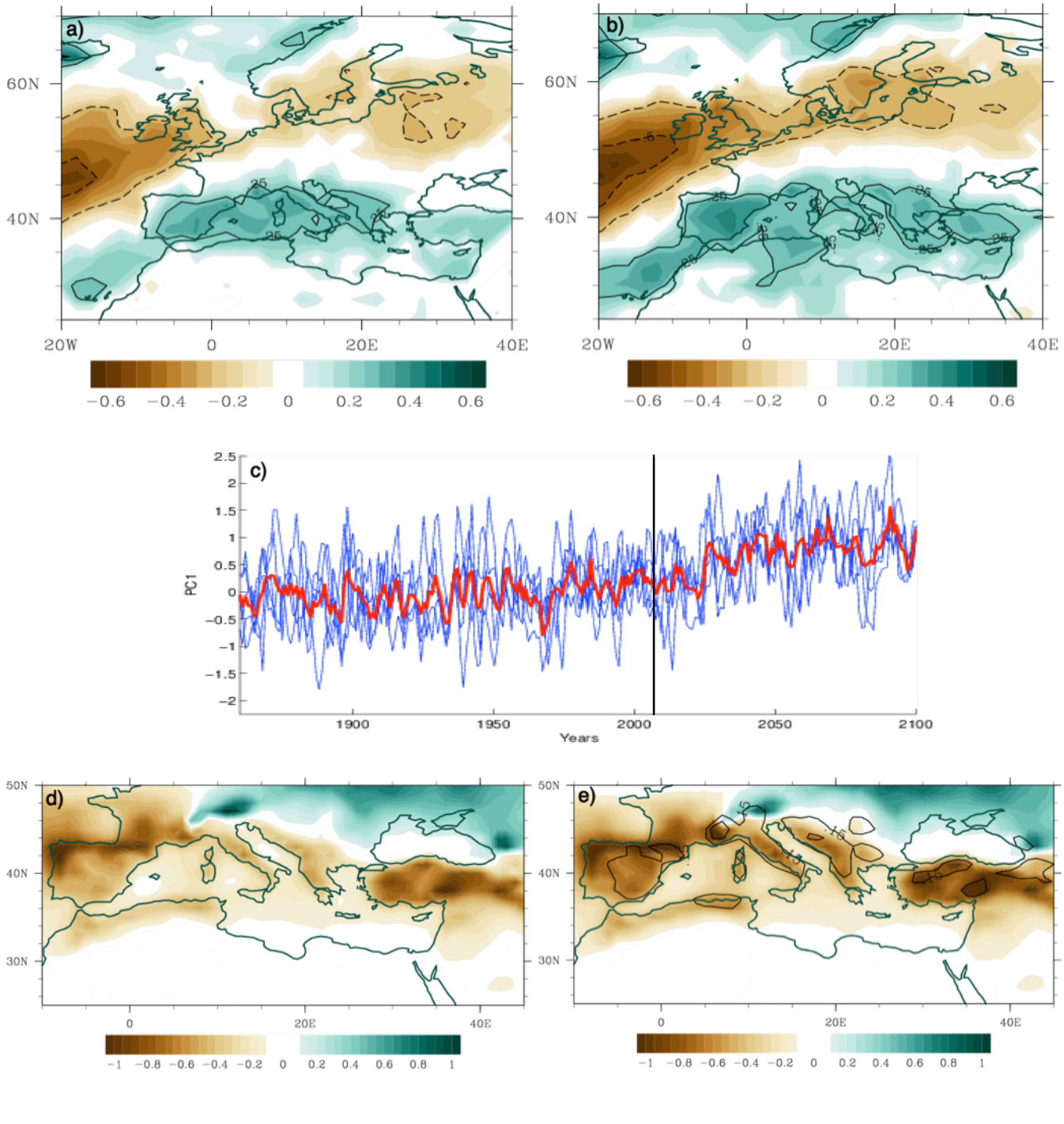

Figure 9. Correlations between the PC1 time series of omega at 500hPa in July and surface atmospheric circulation in the periods (a,c,e) 1960-2010 and (b,d,f) 2050-2100. Correlation values are estimated for a)-b) SLP (shaded and contours), c)-d) meridional wind (shaded and contours), e)-f) precipitation (shaded and contours) and vertically integrated water vapor (contours for the values -0.5, 0.3, 0.5). For a)-d) contours are shown for 0.25 and 0.5 correlation values.

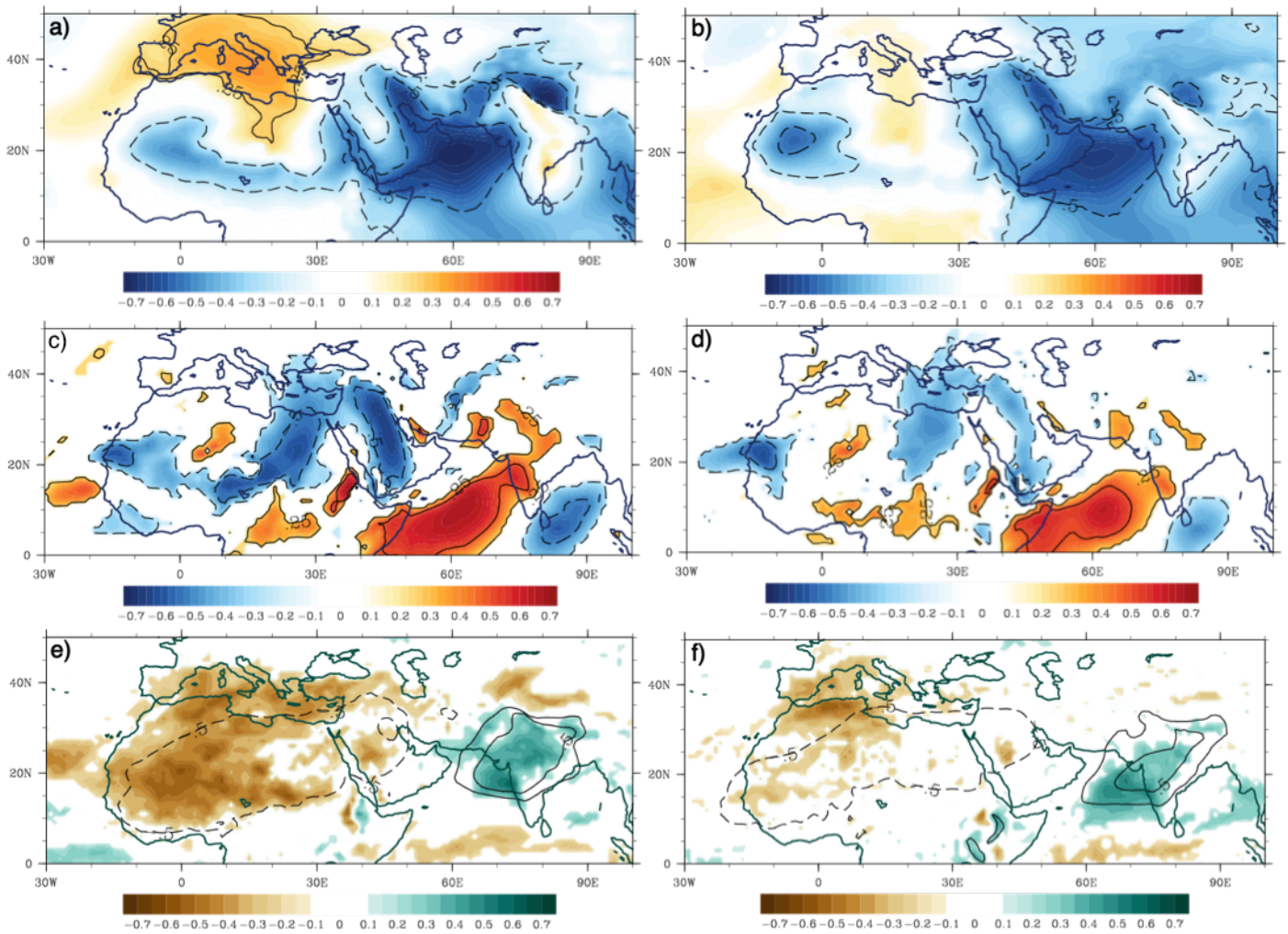

Figure 10. a) Composite differences between the sample with the 300 warmest and 300 coolest seasons over the eastern Mediterranean (30°-36°N, 36°-42°E), for July in the CTRL run, derived from a) surface temperature (°C), and associated differences in b) relative humidity, c) SLP (hPa) and vector wind at 850hpa (m/s), d) height at 850hPa (shaded) and 500hPa (contours), e) omega at 500 hPa, f) precipitation (mm/day).

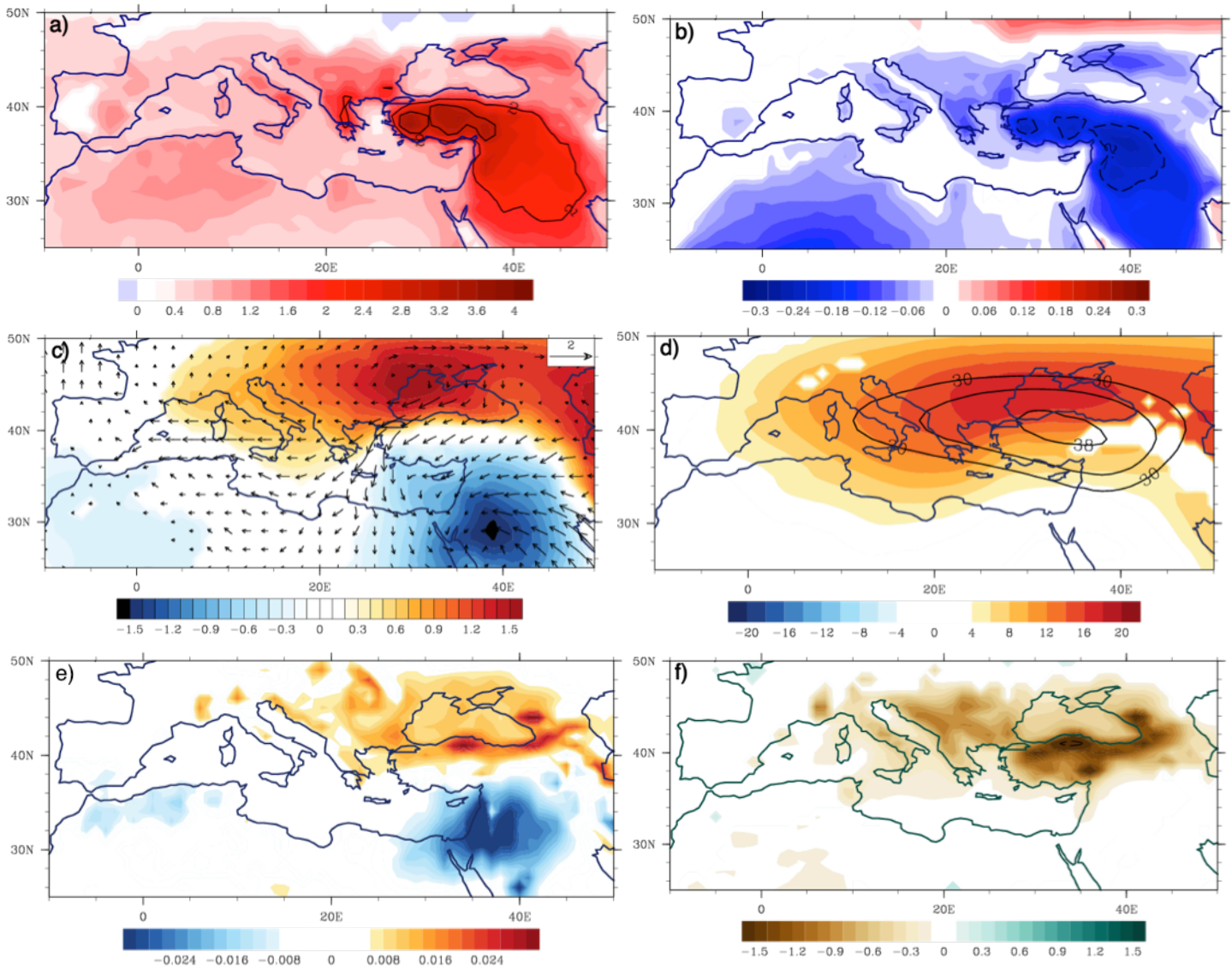

Supplementary Material

Fig SI1. Spatial pattern of SNAO, derived from the 20CR reanalysis, derived from periods: 1851-1890, 1891-1930, 1931-1970, 1971-2010.

Fig SI2. Spatial patterns of the SNAO using SLP, derived from five HIST runs in 1870-1920 (left column), and 1960-2010 (right column). The pattern is shown as correlations between time series of the first PC of SLP and SLP fields in July-August. The sign of each derived EOF is arbitrary, but here the signs were converted to match the SNAO at its negative phase.

Fig SI3. Spatial pattern of SNAO using SLP derived from the period 1970-2030 in the five HIST+PROJ runs. The pattern is shown as correlations between the principal component time series of the first EOF of SLP and SLP fields in July-August.

Fig SI4. Future changes projected for vertical velocities at a) 500 hPa, c) 600 hPa, e) 700 hPa in JJA and in July in b), d), f) respectively. The changes are derived in the period 2061-2099 and compared with the baseline period 1961-1999, derived at the original horizontal resolution (~0.25°). The vertical axis is oriented downward, i.e. negative tendencies (in blue) indicate upward motion while positive tendencies (red, stronger subsidence) indicate downward motion.

Figure SI5. Projected future changes for the summer (JJA) surface temperature (left,°C), and precipitation (right, mm/day) based on the 10-member ensemble simulations of the CSIRO-Mk3-6-0 model, for the forcing scenario RCP8.5.

Fig SI6. As in Fig 9, except that correlations are derived, based on the sample with the 300 coldest (a,b) and 300 warmest (c,d) complete seasons over the eastern Mediterranean in the CTRL run. Correlations are shown for a)-b) meridional wind, c)-d) precipitation.

Fig SI7. As in Fig 10c, except that for a) June, b) August, and for a larger domain.

Fig SI8. As in Fig 10c, except that the regions used for differentiation between warmest and coolest seasons are larger: a) 0°-40°E, 30°-36°N, b) 20°-40°E, 30°-36°N, c) 30°-50°E, 30°-36°N, d) 30°-50°E, 30°-40°N, e) 30°-50°E, 30°-45°N.

Fig SI9. Correlations between the principal component time series of EOF1 omega over EMED and precipitation in (a) June, (b) July (as in Figure 6f), (c) August. Solid lines denote positive correlations, and stippled denote negative correlations, both for the absolute values larger, than 0.25.